

Chongqing University of Posts and Telecommunications
Department of Electrical Engineering

Research on Time-of-Use Tariff of New Energy Power System Considering Supply and Demand Uncertainties

Peng Wang

Submitted in part fulfilment of the requirements for the degree of
Master in Electrical Engineering and
the Diploma of Chongqing University of Posts and Telecommunications, June 2024

Abstract

The uncertainty of supply and demand pose a challenge to the safe and stable operation of the power system and the maintenance of the comprehensive interests. As a price-based demand response (DR) method, time-of-use (ToU) tariff policy guides users to transfer electricity consumption through the difference of peak-valley electricity prices, which can effectively suppress the expansion of the supply-demand power gap and improve the ability of the system to operate economically and safely. This requires the formulation of ToU policy to be reasonable. The main work and contributions of this thesis are as follows:

1. Establish the new energy power system structure and the resource model for supply and demand sides. The supply side includes wind power generation, photovoltaic power generation, gas turbines, and battery energy storage systems. The demand side includes three types of loads: rigid load that cannot be transferred, as well as elastic load and shiftable load that participate in DR. The DR mechanisms of elastic load and shiftable load are modeled based on the demand price elasticity matrix and consumer psychology, respectively. The uncertainty of wind and solar power output is represented by the budget uncertainty set under probability distribution, while the uncertainty of electricity transfer is described by fuzzy membership functions.
2. Build the improved K-Means clustering algorithm to divide peak-valley periods of ToU policy. The original clustering algorithm initializes through the improved membership functions, which models a prior knowledge. Further use gap statistics and data density to determine the optimal initial clustering centers. Finally, fully discuss the potential types of time periods and obtain the period divisions. The problems of manual judgment of clustering number, random initialization, low computational efficiency in traditional clustering algorithms, and insufficient data mining are solved.
3. Build the correction method for abnormal time periods in peak-valley periods division. For load curves with small time scales, there is a problem of rapid changes in load period types during the initial periods division. This period is called abnormal period (AP) and is not conducive to the implementation of ToU policy, so it needs to be corrected. After providing the concept of AP and correction strategies, the corresponding recognition model is constructed to find all the targets to be corrected, and then a correction

model based on fuzzy subsethood is constructed to enable the final period divisions to be available in subsequent optimization models.

4. Build the peak-valley electricity prices optimization model for new energy power systems based on the uncertainty model of supply and demand. A solution model combining the hippo optimization algorithm and CPLEX is proposed to transform the original nonlinear problem into an easily solvable linear problem. Based on typical daily supply and demand data, a case study is conducted to demonstrate that the proposed models can formulate reasonable peak-valley electricity prices to optimize system economics. By adjusting the uncertainty degree, different peak-valley electricity prices and comprehensive benefits can be obtained. Analysis shows that if the power system needs to absorb more wind and solar resources to improve its economics, it is necessary to improve prediction accuracy and robustness. Besides, supply-demand uncertainty can weaken the effect of ToU policy.

Keywords: Time-of-Use Tariff, Clustering Algorithm, Fuzzy Mathematics, Abnormal Periods Correction, Supply-Demand Uncertainty

Acknowledgements

The Chinese version in CNKI provides detailed acknowledgements. But here, I just want to say, to **Yuan**:

We have known each other for a really long time.

My beating heart still makes me love you.

I love you more than I can say.

Although the confession of **I love you** seem pale and powerless.

Let coming years make our love unbreakable.

From Madrid, Spain to Chongqing, China

Contents

Abstract	i
Acknowledgements	iii
1 Introduction	1
1.1 Motivation and background	1
1.2 Thesis structure	3
2 Structure and Models of New Energy Power System	6
2.1 Introduction	6
2.2 Structure of the system	7
2.3 Models of the supply side	8
2.3.1 Wind turbines	8
2.3.2 Photovoltaic systems	9
2.3.3 Gas turbines	10
2.3.4 Battery energy storage systems	10
2.4 Model of the demand side	12

2.4.1	Rigid loads	12
2.4.2	Elastic loads	12
2.4.3	Shiftable loads	13
2.5	Chapter conclusion	14
3	Initial Division of Peak-Valley Periods Based on Improved K-Means Clustering	15
3.1	Introduction	15
3.2	Gap statistics determine the number of clusters	17
3.3	Initial cluster centers based on modified membership functions and data density	18
3.3.1	Initialization based on modified membership functions	19
3.3.2	Initial cluster centers optimization based on data density	24
3.4	Case study	25
3.5	Chapter conclusion	31
4	Abnormal Periods Correction Based on Fuzzy Subsethood	33
4.1	Introduction	33
4.2	Definition of abnormal periods and formulation of correction strategies	34
4.3	Identification model for abnormal periods	36
4.4	Correction model for abnormal periods	37
4.5	Case study	40
4.6	Chapter conclusion	42

5 Modeling of Uncertainty in Supply and Demand Resources	44
5.1 Introduction	44
5.2 Demand side uncertainty modeling	45
5.2.1 Elastic load modeling based on demand price matrix	45
5.2.2 Shiftable load modeling based on consumer psychology	46
5.2.3 Modeling of uncertainty in electricity transfer based on membership function	48
5.3 Supply side uncertainty modeling	49
5.3.1 Probability distribution of wind turbines output	50
5.3.2 Probability distribution of photovoltaic systems output	50
5.3.3 Wind and solar power output modeling based on budget uncertainty set .	51
5.4 Net load modeling based on supply and demand uncertainty resources	53
5.5 Chapter conclusion	54
6 Optimization of Time-of-Use Tariff for the New Energy Power System	55
6.1 Introduction	55
6.2 Time-of-use tariff strategy formulation	56
6.3 Time-of-use tariff optimization model	57
6.3.1 Objective function	58
6.3.2 Constraints	59
6.3.3 Solving model	61
6.4 Case study	63

6.4.1	Simulation settings and instructions	63
6.4.2	Results and analysis of scenario 1	65
6.4.3	Results and analysis of scenario 2	66
6.4.4	Results and analysis of scenario 3	70
6.4.5	Results and analysis of scenario 4	72
6.5	Chapter conclusion	74
7	Conclusion	75
7.1	Summary of thesis achievements	75
7.2	Future work	77
Bibliography		77

List of Tables

3.1	Calculated values of fuzzy parameters a , b , c	26
3.2	Simulation scenarios	28
3.3	Initial cluster centers	28
3.4	Evaluation of clustering quality	31
4.1	Correction strategies for APs	35
4.2	Process of abnormal periods identification model	36
4.3	Process of abnormal periods correction model	39
4.4	Specific time of different periods before and after abnormal periods correction . .	41
4.5	Period types in abnormal periods	42
6.1	Setting of simulation parameters	64
6.2	Scenarios of simulation	64
6.3	Changes in benefits of each link	67
6.4	Changes in electricity consumption during peak-valley periods	68

List of Figures

1.1	Research framework of this thesis.	5
2.1	New energy power system structure.	8
2.2	Temperature-time relationship for dynamic adjustment of air conditioning load.	13
2.3	Power-time relationship for dynamic adjustment of air conditioning load.	13
2.4	Mechanism of time shifts for power consumption in water heaters.	14
3.1	Process of improved K-Means algorithm.	16
3.2	TMF structure for peak-valley periods.	19
3.3	MMF structure for peak periods.	21
3.4	MMF structure for valley periods.	21
3.5	MMF structure for flat periods.	22
3.6	Typical daily load curve.	25
3.7	Statistic parameters under different k	25
3.8	LF values and slopes at different conservative level α	26
3.9	Peak-valley membership degrees under MMF.	27
3.10	Peak-valley membership degrees under TMF.	27

3.11 Iteration process of scenario 1 and scenario 2.	29
3.12 Iteration process of scenario 3 and scenario 4.	29
3.13 Peak-valley periods division result of scenario 1.	29
3.14 Peak-valley periods division result of scenario 2.	30
3.15 Peak-valley periods division result of scenario 3.	30
4.1 Typical structures of APs and NPs.	34
4.2 Distribution characteristics of APs.	34
4.3 Peak-valley periods division before abnormal periods correction.	40
4.4 Peak-valley periods division after abnormal periods correction.	40
5.1 Diagram of load transfer rate function.	47
5.2 Wind speed-probability density distribution curve.	50
5.3 Light intensity-probability density distribution curve.	51
6.1 Framework for time-of-use tariff design mechanism.	57
6.2 Solving model based on the hippopotamus optimization algorithm and CPLEX.	62
6.3 Output range of wind turbines.	63
6.4 Output range of photovoltaic system.	63
6.5 Output of power generation units on the supply side of scenario 1.	65
6.6 Curve of system operation benefits optimization.	66
6.7 Peak-valley electricity prices of each link.	67
6.8 Load curve after time-of-use policy.	68

6.9	Output of each power generation unit in the supply side of scenario 2	69
6.10	Supply side operating costs under different uncertainties.	70
6.11	Prediction error of the output of WT and PV.	71
6.12	Output of each power generation unit with an uncertainty of 0.4.	71
6.13	System comprehensive benefits under different uncertainties.	72
6.14	Peak-valley onto-grid prices under different uncertainties.	73
6.15	Peak-valley transmission-distribution prices under different uncertainties.	73
6.16	Peak-valley selling prices under different uncertainties.	74

Chapter 1

Introduction

This chapter gives the introduction to the thesis, by explaining the motivation for undertaking this task, describing the approach used to tackle the research questions and stating the original contributions of the work presented here.

1.1 Motivation and background

Since the 1970s, many countries and regions have begun to study and implement time-of-use (ToU) policy to address issues such as unstable power systems caused by severe load peak-valley differences [1, 2]. Since the implementation of the reform and opening-up policy of China, although the development of the power industry has lagged behind in some aspects, the electricity consumption patterns of users have become increasingly diversified, and the demand for electricity has shown a rapid growth trend. This trend has kept electricity supply and demand in a tight state for a long time. In order to address the nationwide power shortage problem and alleviate the contradiction between supply and demand sides, the State Council approved and forwarded the "Interim Provisions on Encouraging Fundraising and Implementing Multiple Electricity Prices" proposed by the State Economic Commission and other relevant departments in 1985. The regulation explicitly states that different electricity pricing policies should be implemented for certain types of electricity, including ToU policy. Afterwards, the

government successively issued a series of documents to promote the implementation of ToU policy in various regions, and also introduced seasonal electricity prices and peak electricity prices to cope with the power shortage caused by rapid economic development [3,4].

In the 2020s, as electricity demand continued to grow, power generation companies rapidly developed new energy generation, and the installed capacity of wind and solar power gradually increased. Due to the significant intermittency and volatility of the output of new energy sources such as wind power and photovoltaic power, and with the increasingly complex electricity consumption patterns of power users, the construction and development of new energy power systems need to pay more attention to the balance and coordination of power supply and demand under uncertain factors [5]. With the establishment of the "2020 Dual Carbon Target", China is committed to reducing greenhouse gas emissions and actively exploring the implementation of carbon dioxide reduction and neutralization measures to achieve the goal of net zero emissions. This goal undoubtedly poses higher requirements and challenges for the construction and development of new energy systems [6,7]. In 2021, there was a nationwide electricity shortage, and many regions had to implement measures such as power rationing and off peak electricity consumption, resulting in a significant increase in electricity market transaction prices. To effectively address these challenges, the National Development and Reform Commission has issued a notice requiring all regions to further optimize and improve the ToU policy, fully consider factors such as new energy grid connection, load characteristics, scientifically and reasonably determine the peak-valley electricity prices, and peak-valley periods to ensure the stable operation and sustainable development of the electricity market.

Demand response is a power system management strategy aimed at reducing or transferring electricity load during peak hours by changing the electricity consumption behavior of power users. It mainly uses electricity price signals or other incentive measures to guide users to reduce electricity consumption during peak hours, thereby improving the economics and reliability of the power system [8–11]. The ToU policy guides users to adjust their electricity consumption time by setting different electricity prices, to achieve peak shaving and valley filling [12], increase the load rate of the power system [13], thereby alleviating the contradiction between supply and demand, and reducing power outages and restrictions. In addition, ToU policy can improve

the operational efficiency of power generation equipment, optimize resource allocation [14], promote the consumption and utilization of new energy [15,16], reduce environmental pollution, promote the development of emerging industries such as energy storage and distributed power generation [17–20], and further improve the reliability of power supply [21].

The supply-demand uncertainty has a significant impact on the stable operation of the power system and the economics of the electricity market [22]. As the proportion of wind and solar power gradually increases, the output from the supply side is increasingly affected by natural factors such as wind speed and light intensity, leading to an increase in wind and solar prediction errors. Therefore, the scheduling and operation of the power system are facing unprecedented challenges [23]. The diversity of daily electricity consumption also creates uncertainty on the demand side. Therefore, in the research of power system scheduling, it is necessary to consider the uncertainty, which can ensure the stability and safety of the power system [24], optimize resource allocation and operation management [25], promote the sustainable use of renewable energy [26], support the healthy development of the electricity market.

In summary, considering the uncertainty, in order to fully utilize the ToU policy, it is necessary to scientifically and reasonably divide peak-valley periods and formulate peak-valley electricity prices. The current time periods division method has problems such as human judgment, difficulty in determining the type of time period at boundary moments, and difficulty in obtaining the optimal time periods division, which cannot guarantee the implementation effect of ToU policy. This thesis aims to establish a model to solve the above problems.

1.2 Thesis structure

The key factors in the formation of ToU policy are the reasonable division of peak-valley periods and the formulation of electricity prices. This thesis considers the supply-demand uncertainty and aims to maximize the comprehensive benefits of supply, grid and demand sides. It formulates peak-valley electricity prices for different links and discusses the economic impact of ToU policy on the operation of the power system. The main research framework and

logical relationship are shown in Figure 1.1.

Chapter 1. Introduction. A brief introduction is given to the research content and chapter arrangement of this thesis.

Chapter 2. Structure and models of new energy power system. Build the structure of the new energy power system in this thesis, which includes three links: the supply side includes wind turbines, photovoltaic power generation systems, gas turbines, and battery energy storage systems; The demand side includes rigid load, elastic load, and shiftable load; The grid side includes the transmission and the distribution network. This chapter explains the characteristics of different links based on typical models and provides corresponding mathematical models.

Chapter 3. Initial division of peak-valley periods based on improved K-Means clustering algorithm. Adopting an improved K-Means clustering algorithm to partition initial peak-valley periods, this improvement overcomes the random initialization of traditional K-Means and the artificially given number of clusters. The gap statistic is used to determine the optimal number of time period types. Improve the membership function for initializing peak, flat, valley clustering centers. If the optimal number of time period types is not met, search for new initial clustering centers based on data density. Finally, the K-Means clustering algorithm is used to divide peak-valley periods.

Chapter 4. Abnormal periods correction. For the daily load curve with a small time scale of 5 minutes as an example, the initial partitioning results of the K-Means clustering algorithm may encounter the problem of rapid changes in the type of load period in a short period of time, which is called an abnormal period. Develop corresponding correction strategies and recognition models for different abnormal periods, and finally build a correction model to correct all abnormal periods, so that the peak-valley periods division results can support the subsequent formulation of electricity prices.

Chapter 5. Modeling of supply-demand uncertainty. Firstly, the demand response modes of different loads and the probability distribution of wind and solar power are modeled and explained separately. Then, the membership function is used to characterize the uncertainty

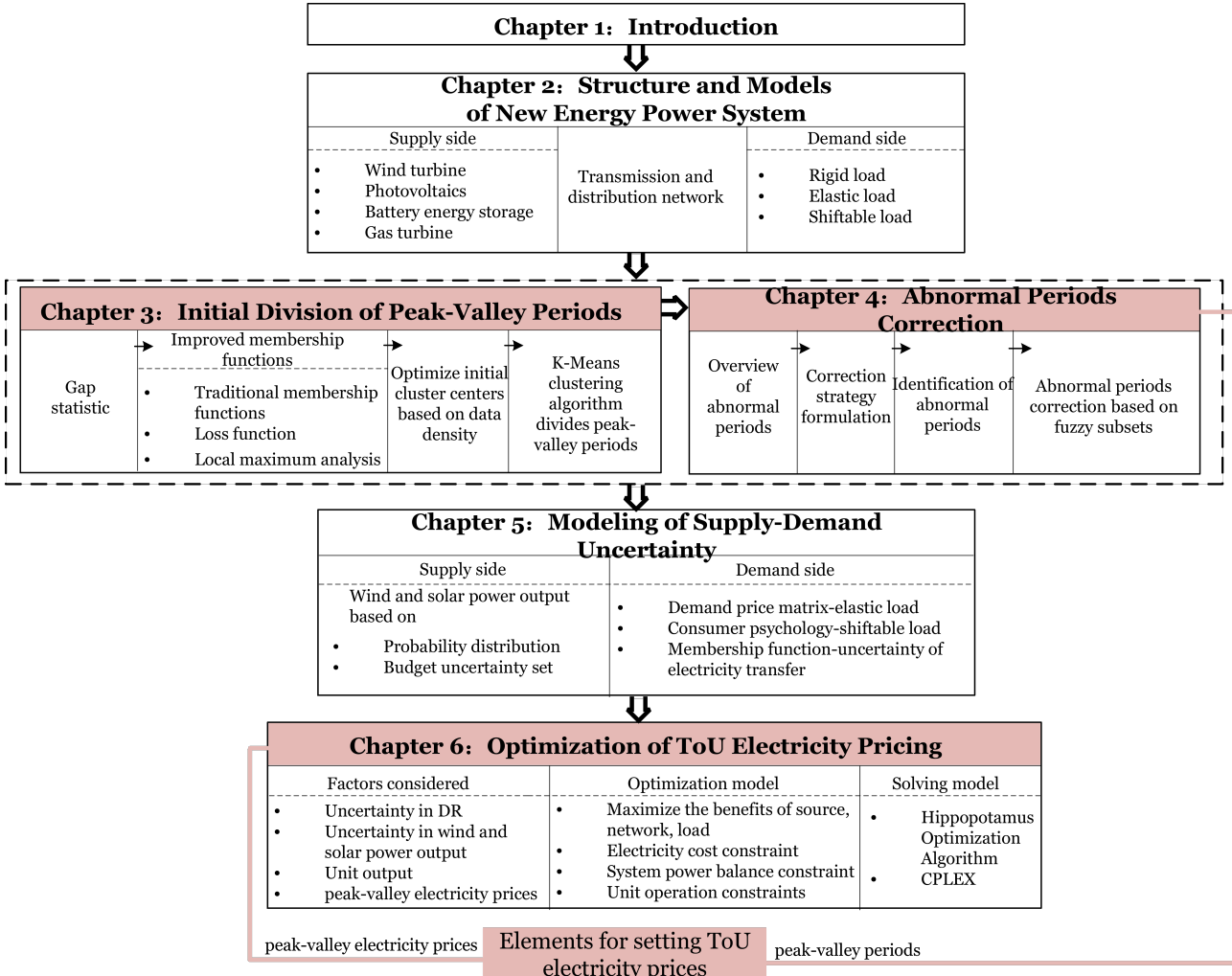


Figure 1.1: Research framework of this thesis.

of electricity transfer, and the uncertainty of wind and solar power is modeled using a budget uncertainty set combined with the probability distribution.

Chapter 6. Optimization of ToU electricity pricing. Construct a ToU electricity prices optimization model for new energy power systems based on supply-demand uncertainty, with the goal of achieving comprehensive benefits in system operation. Establish a solution model combining hippopotamus optimization algorithm and CPLEX to transform the original non-linear programming problem into a linear programming problem for solving. Then, adjust the uncertainty of supply and demand and explore the coupling relationship between ToU tariff, supply-demand uncertainty, and system operation economics.

Chapter 7. Summary and prospect. Summarize the research work of this thesis and propose future research prospects.

Chapter 2

Structure and Models of New Energy Power System

2.1 Introduction

The feature of a new energy power system structure is that it includes various power sources, including renewable energy. For example, wind turbines (WTs), photovoltaic systems (PVs), gas turbines (GTs), and battery energy storage systems (BESS), all belong to distributed generations (DGs) in the new energy power system. According to their respective output characteristics and control methods, they can be classified into two types: uncontrollable DGs and controllable DGs. Among them, WTs and PVs are classified as uncontrollable due to their randomness and volatility. This type of DGs alone cannot ensure the safe and stable operation of the new energy power system. GTs, BESS, etc. belong to controllable DGs due to their controllable output power. They can adjust their output in a timely manner according to the power changes of the new energy power system, maintaining the stable operation of the system. In the process of power transmission, the new energy power system utilizes high-voltage transmission technology to transport electricity from power plants to various electricity consuming areas. In the allocation process, the new energy power system distributes electricity reasonably to various electrical equipment based on the needs and characteristics of users,

meeting their demands.

The new energy power system plays a crucial role in energy transition and sustainable development. This chapter constructs the structure and models of the new energy power system, and elaborates on the analysis of the characteristics of different power generation units on the supply side and different flexible loads on the demand side, laying a solid foundation for the subsequent modeling of supply-demand uncertainty and the establishment of time-of-use electricity price optimization models.

2.2 Structure of the system

On the supply side, the output of WTs and PVs is largely influenced by wind speed and light intensity, both of which have significant randomness and intermittency. Therefore, the output of wind and solar power often presents significant uncertainty and is difficult to accurately predict and regulate. To maintain the safe and reliable operation of the system, stable power sources such as GTs and BESS are required to be connected to the power system.

The demand side includes three types of loads: rigid loads, elastic loads, and shiftable loads. Rigid loads do not transfer electricity usage time periods, while flexible loads such as elastic loads and shiftable loads will respond to time-of-use electricity pricing policies, obey price signals from different time periods, adjust electricity usage plans, reduce peak-valley differences, and improve system economy and safety.

To maintain the supply-demand balance of the power system, the power grid will transport the electricity output from the supply side to the distribution network according to the supply and demand situation, and distribute it to different electricity loads as needed.

Based on the above analysis and explanation, the structure of the new energy power system in this thesis is shown in Figure 2.1.

The following content provides a detailed explanation of the supply and demand characteristics of different power generation units on the supply side and different loads on the demand

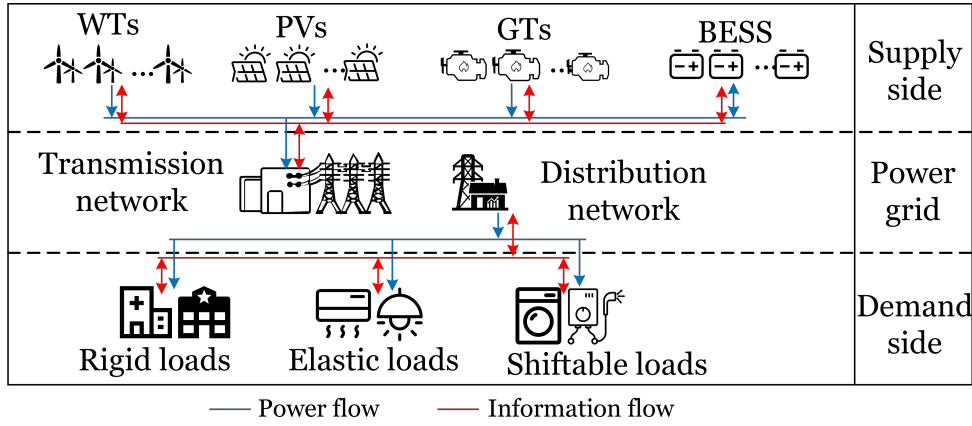


Figure 2.1: New energy power system structure.

side, and cites classical models for analysis.

2.3 Models of the supply side

The supply side models include WTs and PVs with uncertainty, as well as GTs and BESS with stable output. Clarifying the characteristics of wind and solar power output is helpful for subsequent uncertainty modeling, while for deterministic output equipment, corresponding operation maintenance cost-output power functions and operating constraints are provided.

2.3.1 Wind turbines

The core operating mechanism of WTs is to use wind power to rotate the windmill blades, thereby increasing the rotational speed. This process efficiently converts mechanical energy into electrical energy through electromagnetic induction effect. Among the many factors that affect the output of WTs, the wind speed is particularly critical. Ignoring the nonlinear factors that have a smaller impact, a direct relationship between the output of WTs and wind speed can be clearly established. Use a simplified piecewise linear function to describe it [27], as

shown in (2.1).

$$P_{\text{WT}}(t) = \begin{cases} 0, & \text{if } v_t < v_{ci} \text{ or } v_t > v_{co} \\ P_{\text{WT,r}} \cdot \frac{v_t - v_{ci}}{v_r - v_{ci}}, & \text{if } v_{ci} \leq v_t \leq v_r \\ P_{\text{WT,r}}, & \text{if } v_r < v_t \leq v_{co} \end{cases} \quad (2.1)$$

Where, v_{ci} , v_{co} , and v_r are the cut-in wind speed, cut-out wind speed, and rated wind speed, respectively. $P_{\text{WT,r}}$ is the rated power of the WT. $P_{\text{WT}}(t)$ is the actual output of the WT during the time period t .

During the operation of the system, the maintenance cost of the WT is represented by (2.2).

$$C_{\text{WT}}(t) = \lambda_{\text{WT}} \cdot P_{\text{WT}}(t) \cdot \Delta t \quad (2.2)$$

Where, λ_{WT} is the maintenance cost coefficient, CNY/kW.h, Δt is the scheduling step.

2.3.2 Photovoltaic systems

The core principle of PVs is to effectively convert solar radiation into electrical energy by utilizing the photovoltaic effect at the semiconductor interface. Subsequently, through the action of the inverter, direct current is converted into alternating current to meet the daily electricity needs of users. Similar to WTs, ignoring the uncertain nonlinear factors, the output of PVs is mainly related to the intensity of light, also showing a linear relationship [27], as shown in (2.3).

$$P_{\text{PV}}(t) = L_i(t) \cdot S_{\text{PV}} \cdot \eta_{\text{PV}} \quad (2.3)$$

Where, $L_i(t)$ is the light intensity during the time period t . S_{PV} is the total area of the photovoltaic array. η_{PV} is the photoelectric conversion efficiency.

During the operation of the new energy power system, the maintenance cost of the PV is represented by (2.4).

$$C_{\text{PV}}(t) = \lambda_{\text{PV}} \cdot P_{\text{PV}}(t) \cdot \Delta t \quad (2.4)$$

Where, λ_{PV} is the maintenance cost coefficient, CNY/kW.h.

2.3.3 Gas turbines

GTs are an important support for new energy power systems to ensure the safe and reliable operation. The operation and maintenance cost is represented by (2.5) [28].

$$C_{GT}(t) = [\lambda_{GT,1} \cdot P_{GT}(t) + \lambda_{GT,2}] \cdot \Delta t \quad (2.5)$$

Where, $C_{GT}(t)$ represents the operation and maintenance cost of the GT during the time period t . $\lambda_{GT,1}$ and $\lambda_{GT,2}$ are the operation and maintenance cost parameters, with units of CNY/kW.h and CNY/h respectively. $P_{GT}(t)$ is the actual output of the GT during the time period t .

The output power constraint of the GT is shown in (2.6).

$$P_{GT}^{\min} \leq P_{GT}(t) \leq P_{GT}^{\max} \quad (2.6)$$

Where, P_{GT}^{\max} and P_{GT}^{\min} respectively represent the maximum and minimum output of the GT.

The ramping constraint of the GT is shown in (2.7).

$$P_{ramp}^{\min} \leq |P_{GT}(t) - P_{GT}(t-1)| \leq P_{ramp}^{\max} \quad (2.7)$$

Where, P_{ramp}^{\max} and P_{ramp}^{\min} respectively represent the maximum ramp rate and minimum ramp rate of the output power of the GT.

2.3.4 Battery energy storage systems

During the operation of the power system, the BESS will charge and convert electrical energy into chemical energy for storage; When the power system requires additional electricity, the BESS converts the stored chemical energy back into electrical energy through the discharge

process to meet the load demand. The cost mainly focuses on the initial investment cost and subsequent operation and maintenance costs [28], and the average charging and discharging cost during the time period t is represented by (2.8).

$$C_{\text{BESS}}(t) = \lambda_{\text{BESS}} \cdot [P_{\text{BESS}}^{\text{dis}}(t)/\eta_{\text{BESS}} + P_{\text{BESS}}^{\text{ch}}(t) \cdot \eta_{\text{BESS}}] \cdot \Delta t \quad (2.8)$$

Where, λ_{BESS} is the unit charge and discharge cost coefficient, CNY/kW.h. $P_{\text{BESS}}^{\text{ch}}$ and $P_{\text{BESS}}^{\text{dis}}$ respectively represent the charging and discharging power of the BESS during the time period t . η_{BESS} is the charging and discharging efficiency. During operation, constraints must be satisfied as shown in (2.9), (2.10), (2.11), (2.12).

$$0 \leq P_{\text{BESS}}^{\text{ch}}(t) \leq [1 - U_{\text{BESS}}(t)] \cdot P_{\text{BESS}}^{\text{max}} \quad (2.9)$$

$$0 \leq P_{\text{BESS}}^{\text{dis}}(t) \leq U_{\text{BESS}}(t) \cdot P_{\text{BESS}}^{\text{max}} \quad (2.10)$$

$$\eta_{\text{BESS}} \cdot \sum_{t=1}^T P_{\text{BESS}}^{\text{ch}}(t) \cdot \Delta t - \frac{1}{\eta_{\text{BESS}}} \cdot \sum_{t=1}^T P_{\text{BESS}}^{\text{dis}}(t) \cdot \Delta t = 0 \quad (2.11)$$

$$E_{\text{BESS}}^{\min} \leq E_{\text{BESS}}^0 + \eta_{\text{BESS}} \cdot \sum_{t'=1}^t P_{\text{BESS}}^{\text{ch}}(t') \cdot \Delta t - \frac{1}{\eta_{\text{BESS}}} \cdot \sum_{t'=1}^t P_{\text{BESS}}^{\text{dis}}(t') \cdot \Delta t \leq E_{\text{BESS}}^{\max} \quad (2.12)$$

Where, (2.9) and (2.10) represent the constraints of charging and discharging power. $P_{\text{BESS}}^{\text{max}}$ is the maximum charging and discharging power. $U_{\text{BESS}}(t)$ is a parameter ranging from 0 to 1, indicating the charging and discharging status of the BESS: 1 indicates discharge, 0 indicates charging. (2.11) ensures that the capacity of the BESS is equal at the beginning and end of the scheduling process, ensuring that it can effectively participate in the system cycle scheduling. (2.12) is the constraint on the remaining capacity of the BESS, where E_{BESS}^0 is the initial capacity, E_{BESS}^{\max} and E_{BESS}^{\min} are the maximum and minimum remaining capacities, respectively. This constraint aims to prevent overcharging and overdischarging of the BESS and avoid damaging the battery life.

2.4 Model of the demand side

The demand side model includes rigid loads, elastic loads, and shiftable loads. This section cites typical types of loads in actual production and life to explain the characteristics of electricity transfer. To lay the foundation for modeling demand response (DR) and its uncertainty.

2.4.1 Rigid loads

Rigid loads mainly include loads from certain important national production sectors, which are basically not affected by usual load factors and their power remains at a fixed level. Typical rigid loads include residential loads such as refrigerators and departments such as healthcare and military affairs. These requirements are rigid and will not change due to DR. Rigid loads have a significant impact on production and our daily life, with high priority and no participation in DR, so the electricity consumption time will not be transferred. If the electricity demand of rigid loads cannot be met, it may affect the normal life of residents and even cause power supply accidents, causing huge losses to society.

2.4.2 Elastic loads

Elastic loads have the characteristics of being easy to save and replace. Specifically, when facing changes in electricity prices, power users often choose to save some load, increase electricity consumption, or engage in substitution behavior between electricity and other energy sources. These response behaviors reflect the flexibility and adjustability of elastic loads. Typical electrical equipment includes air conditioning and lighting devices. The working state of summer air conditioning load is analyzed below to further understand this characteristic [29], and its dynamic adjustment process is shown in Figures 2.2 and 2.3.

From Figures 2.2 and 2.3, it can be seen that as electricity prices rise, users tend to reduce the power of air conditioning loads, resulting in a gradual increase in indoor temperature. However, after a period of time, the air conditioning load power will rebound until the indoor

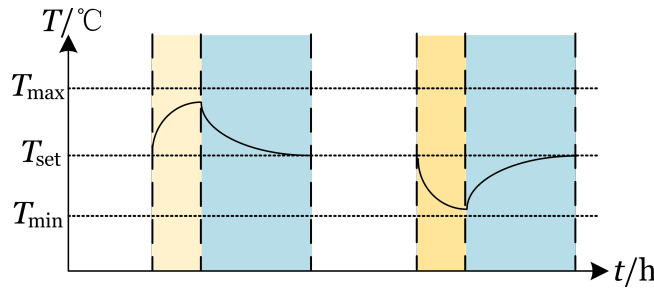


Figure 2.2: Temperature-time relationship for dynamic adjustment of air conditioning load.

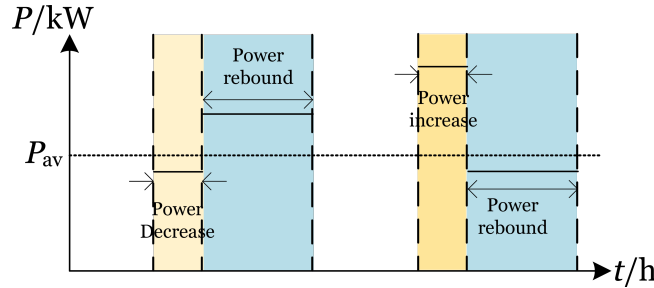


Figure 2.3: Power-time relationship for dynamic adjustment of air conditioning load.

temperature returns to the set temperature value T_{set} . Similarly, when electricity prices are lowered, users tend to increase air conditioning power, causing the indoor temperature to decrease and eventually stabilize back to the set temperature T_{set} . With the collection of electricity fees at different time periods, users will adjust the start and end time and operating status of air conditioners economically and flexibly, which enables the elastic load represented by air conditioners to have the function of peak shaving and valley filling.

2.4.3 Shiftable loads

The shiftable loads are easy to transfer. When the electricity consumption period is affected by factors such as power dispatch instructions and changes in electricity prices, they will be shifted, that is, the load originally planned to be used in one time period will be adjusted to be used in another time period. The total load of this translation remains unchanged, only the usage period has changed. Faced with changes in electricity prices, power users usually spontaneously adjust the allocation of some loads at different times to respond to changes in electricity prices, such as washing machines and water heaters. Taking the working state of a water heater as an example, the mechanism of transferring current work tasks to other time

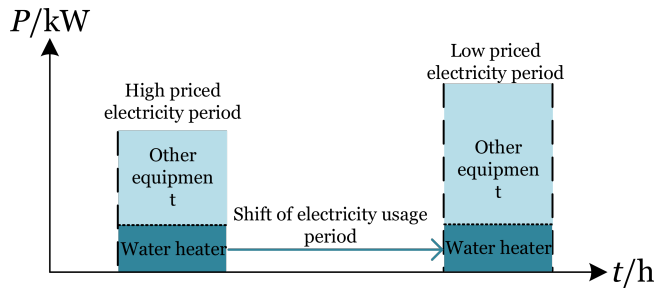


Figure 2.4: Mechanism of time shifts for power consumption in water heaters.

periods is shown in Figure 2.4.

In the situation shown in Figure 2.4, the water heater exhibits flexible load shifting characteristics by adjusting its working time from high electricity price periods to low electricity price periods while maintaining the same workload. At the same time, other devices, including non interruptible devices, will also adjust their working status accordingly with the reduction of electricity charges.

2.5 Chapter conclusion

This chapter introduces the researched new energy power systems, including wind turbines, photovoltaic systems, gas turbines, and battery energy storage systems; The demand side includes rigid loads, elastic loads, and shiftable loads. Firstly, the relationship between natural resources, new energy output, and operation and maintenance costs of wind and solar power is elaborated. Subsequently, the operation and maintenance cost-output relationship and related constraints of gas turbines and battery energy storage systems are elaborated. For the demand side, typical equipment such as air conditioning and water heaters are used to characterize the characteristics of elastic loads and shiftable loads, respectively.

Chapter 3

Initial Division of Peak-Valley Periods Based on Improved K-Means Clustering

3.1 Introduction

Clustering algorithm is a typical time-of-use periods partitioning method. Its basic idea is to iteratively partition the dataset into multiple different clusters, so that data objects within the same cluster are as similar as possible, while data objects between different clusters are as different as possible. This is consistent with the idea of peak-valley periods partitioning, that is, load power within the same time period type is as similar as possible, and load power similarity between different time period types is maximized. Therefore, clustering algorithms can consider the numerical relationship between load power at different times and effectively divide peak-valley periods for different load curves.

The K-Means clustering algorithm is the most commonly used method for dividing peak-valley periods, but it has common problems with traditional clustering algorithms, such as the number of clusters being given based on human experience and the cluster centers being

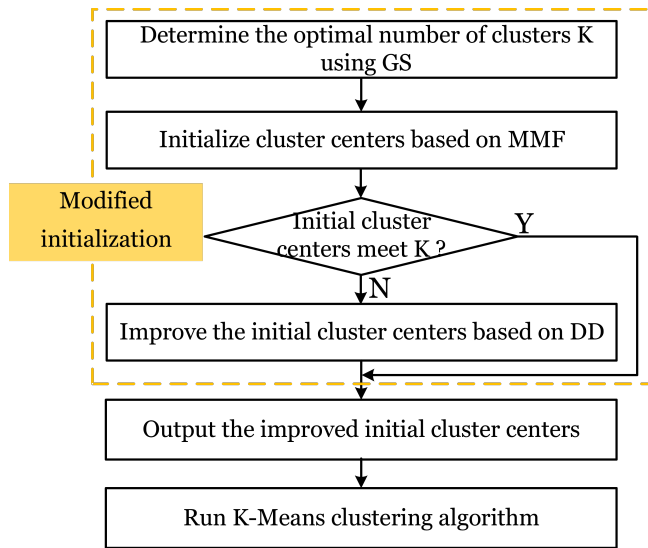


Figure 3.1: Process of improved K-Means algorithm.

randomly initialized. This not only leads to random clustering results, poor clustering efficiency, but also makes it difficult to effectively mine the numerical characteristics of the load curve.

This chapter proposes an improved K-Means clustering algorithm to address the problem of insufficient determination of the initial cluster centers in traditional clustering algorithms. The improvement of the algorithm mainly combines the modified membership functions (MMF), gap statistics (GS), and data density (DD). The algorithm framework is shown in Figure 3.1.

The specific steps are as follows:

Step 1: Determine the optimal number of clusters K for the dataset using GS.

Step 2: Construct the MMF to initialize the clustering centers.

Step 3: If the cluster centers initialized by the MMF satisfy the optimal number of clusters K , output the cluster centers directly and run the K-Means clustering algorithm to divide the peak-valley periods.

Step 4: If the cluster centers initialized by the MMF do not meet the optimal number of clusters K , then search for new initial cluster centers based on DD until the K is met. Finally, run the K-Means clustering algorithm to divide the peak-valley periods.

The principle of the K-Means algorithm used to divide peak-valley periods is as follows:

Step 5: Calculate the distance between each data sample x_t and different initial cluster centers

(v_1, v_2, \dots, v_k) . Then divide it into clusters with the shortest distance, as shown in (3.1).

$$x_t \in c_j, \quad \text{if} \quad d(x_t, v_j) < d(x_t, v_i) \quad (3.1)$$

Where, $d(x_t, v_j)$ is the distance from the data sample x_t to the cluster center v_j .

Step 6: Calculate the mean value within each cluster c_j and use it as the new cluster center, as shown in (3.2).

$$v_j = \frac{1}{|c_j|} \cdot \sum_{x_t \in c_j} x_t \quad (3.2)$$

Where, v_j is the cluster center of cluster c_j . x_t is the data within cluster c_j .

Step 7: Repeat **Steps 5-6** until the objective function converges to the minimum value as shown in (3.3).

$$J = \min \sum_{j=1}^k \sum_{x_t \in c_j} |x_t - v_j|^2 \quad (3.3)$$

3.2 Gap statistics determine the number of clusters

The GS is used to determine the optimal number of clusters K based on the comparison of the degree of dispersion between the dataset and the dataset generated by the reference distribution [30]. The detailed steps of this model are as follows:

Step 1: Use the K-Means clustering algorithm to divide the dataset into k clusters: c_1, c_2, \dots, c_k , and calculate the sum of squared distances D_r between samples within each clusters, as shown in (3.4).

$$D_r = \sum_{x_i \in c_r} \sum_{x_j \in c_r} |x_i - x_j|^2 \quad (3.4)$$

Where, x_i and x_j are data samples within cluster c_r .

Step 2: Obtain the compactness $W(k)$ by normalizing and summing D_r , as shown in (3.5).

$$W(k) = \sum_{r=1}^k \frac{1}{2 \cdot |c_r|} \cdot D_r \quad (3.5)$$

Step 3: Construct the gap statistics $Gap(k)$ using (3.6).

$$Gap(k) = E^*\log(W(k)) - \log(W(k)) \quad (3.6)$$

Where, $E^*\log(W(k))$ is the expected value of $\log(W(k))$, which is estimated by using the logarithmic mean of $W_b^*(k) \sim U(\min(x), \max(x))$, as shown in (3.7).

$$E^*\log(W(k)) = \frac{1}{B} \cdot \sum_{b=1}^B \log(W_b^*(k)) \quad (3.7)$$

Where, B is the number of reference datasets. According to the law of large numbers, when B is sufficiently large, the error caused by the randomness of the K-Means clustering algorithm can be ignored.

Step 4: Calculate the standard deviation $sd(k)$ as shown in (3.8).

$$sd(k) = \sqrt{\frac{1}{B} \cdot \sum_{b=1}^B (\log(W_b^*(k)) - E^*\log(W(k)))^2} \quad (3.8)$$

Step 5: Select the k_{min} that satisfies (3.9) and (3.10) to determine the optimal number of clusters K.

$$Gap(k) \geq Gap(k+1) - s_{k+1} \quad (3.9)$$

$$s_k = \sqrt{\frac{1+B}{B}} \cdot sd(k) \quad (3.10)$$

After determining the optimal number of clusters K, only the values of the initial cluster centers need to be calculated to complete the initialization.

3.3 Initial cluster centers based on modified membership functions and data density

Firstly, improve the traditional membership functions (TMF) and generate initial cluster centers. If the optimal number of clusters K is not met, then search for new cluster centers based

on DD to complete cluster centers initialization.

3.3.1 Initialization based on modified membership functions

In the study of time-of-use policy, fuzzy membership functions can be divided into three categories: large, small, and middle. They are used to describe the correlation between load power and peak-valley periods [31]. The structure of TMF is shown in Figure 3.2.

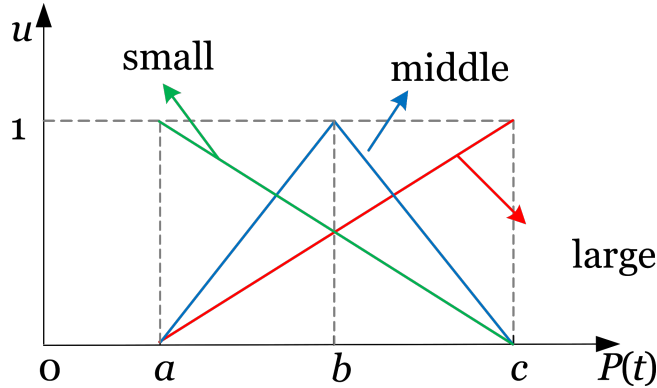


Figure 3.2: TMF structure for peak-valley periods.

Where, a , b , and c represent the minimum, mean, and maximum values of the load power curve, respectively. u is the peak-valley membership degree. When the power value is equal to a , the small membership degree is equal to 1, and the corresponding period must be a valley period; When the power value is equal to c , the large membership degree is equal to 1, and the corresponding period must be in the peak period; When the power value is equal to b , the middle membership degree is equal to 1, and the corresponding period must be the flat period. For other power values, calculate their membership degrees according to Figure 3.2.

According to the above calculation, the peak-valley membership matrix \mathbf{U} can be obtained, as shown in (3.11).

$$\mathbf{U} = \begin{bmatrix} u_1^p & u_2^p & \dots & u_T^p \\ u_1^f & u_2^f & \dots & u_T^f \\ u_1^v & u_2^v & \dots & u_T^v \end{bmatrix} \quad (3.11)$$

Where, u_t^p , u_t^f , u_t^v are the membership degrees of the power values during the t period, which belong to the peak period, flat period, and valley period, respectively. T is the length of the

scheduling cycle.

The sum of membership degrees must be equal to 1, therefore \mathbf{U} must be normalized by constraint (3.12) in order to be applicable to clustering.

$$\text{s.t. } \sum_{k=1}^3 u_t^k = 1, \quad 0 \leq u_t^k \leq 1 \quad (3.12)$$

Based on the membership degree above, calculate the initial cluster center v_k using (3.13).

$$v_k = \frac{\sum_{t=1}^T (u_t^k)^2 \cdot P(t)}{\sum_{t=1}^T (u_t^k)^2} \quad (3.13)$$

Although TMF can easily and quickly calculate the peak-valley membership of any load curve and obtain initial cluster centers, the single setting of fuzzy parameters a , b , and c ignores a prior knowledge: it is possible to judge the peak-valley period of load power in a certain interval in advance based on experience. This neglect leads to the initial clustering centers being only able to stabilize the clustering process and results, but cannot optimize computational efficiency. The improvement of the TMF fully considers the characteristics of the load curve, and its specific advantages are as follows.

This thesis uses a semi trapezoidal membership function to calculate the membership degree during peak periods, as shown in (3.14) and Figure 3.3.

$$u_t^p = \begin{cases} 0, & \text{if } P(t) < b \\ \frac{P(t)-a}{c-a}, & \text{if } b \leq P(t) < c \\ 1, & \text{if } P(t) \geq c \end{cases} \quad (3.14)$$

Where, since the power smaller than parameter b , i.e. the mean of the power curve, cannot belong to the peak period, the peak period membership degree of $[a, b]$ is no longer calculated. In addition, a and c here are no longer the minimum and maximum values of load power.

Similarly, the MMF for valley periods is shown in Figure 3.4 and (3.15). Since power values greater than parameter b do not belong to valley periods, the membership degree of valley

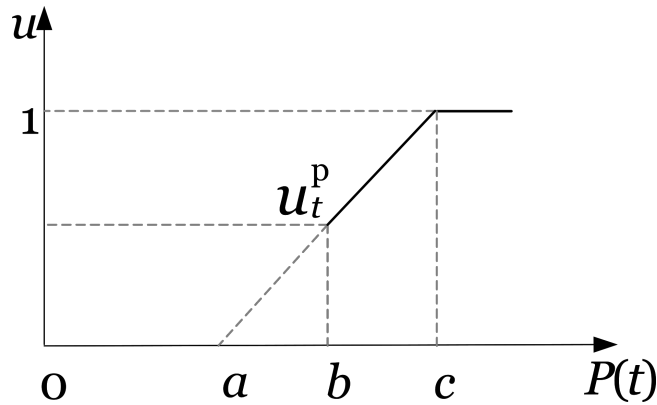


Figure 3.3: MMF structure for peak periods.

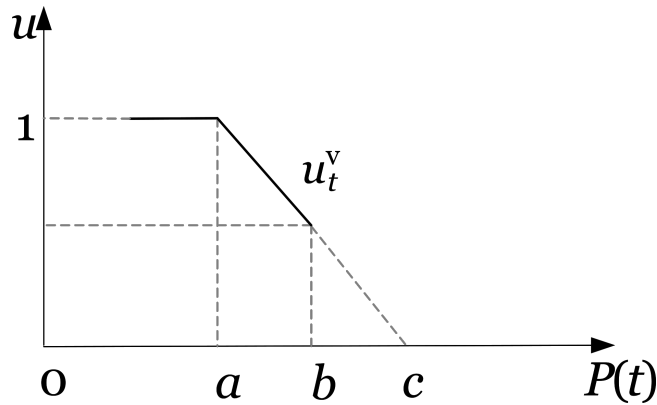


Figure 3.4: MMF structure for valley periods.

periods within $[b, c]$ is not considered.

$$u_t^v = \begin{cases} 1, & \text{if } P(t) < a \\ \frac{c-P(t)}{c-a}, & \text{if } a \leq P(t) < b \\ 0, & \text{if } P(t) \geq b \end{cases} \quad (3.15)$$

The MMF for the flat period is a triangle, as shown in Figure 3.5 and (3.16). From Figures 3.3 and 3.4, it can be seen that the peak membership degree for power values greater than c is 1, and the valley membership degree for power values less than a is 1. Therefore, only the membership degree of the flat segment within $[a, c]$ is considered here.

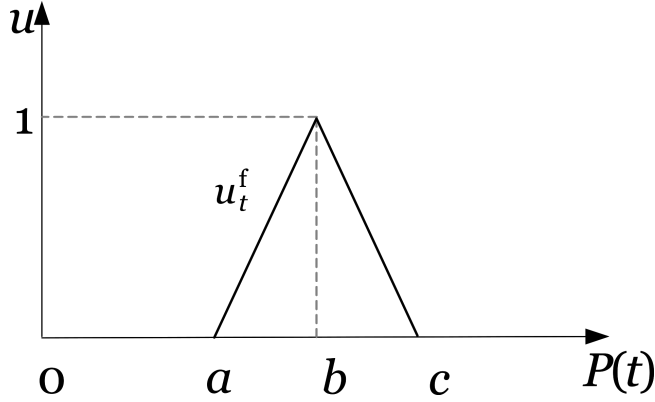


Figure 3.5: MMF structure for flat periods.

$$u_t^f = \begin{cases} 0, & \text{if } P(t) < a \\ \frac{P(t)-a}{b-a}, & \text{if } a \leq P(t) < b \\ \frac{c-P(t)}{c-b}, & \text{if } b \leq P(t) < c \\ 0, & \text{if } P(t) \geq c \end{cases} \quad (3.16)$$

Compared with the TMF that blur the entire load curve, some intervals of the MMF are clear. Obviously, TMF are more conservative because they consider the possibility of peak, flat, and valley power values at all times of the load curve, while MMF assume that power values in a specific interval can only belong to one period type. In practical engineering, these intervals are determined based on experience and prior knowledge. In this thesis, TMF are considered the most conservative, while MMF are more risky. The fuzzy parameters a , b , and c are calculated using (3.17).

$$\begin{cases} a = \min(P(t)) + (1 - \alpha) \cdot (\max(P(t)) - \min(P(t))) \\ c = \max(P(t)) - (1 - \alpha) \cdot (\max(P(t)) - \min(P(t))) \\ b = (a + c)/2 \end{cases} \quad (3.17)$$

Where, b is the mean value of the load curve. $\alpha \in [0, 1]$ is the degree of conservatism. The larger the α is, the closer a and c are to the minimum and maximum load power, and the more conservative the MMF is; The smaller the α is, the less conservative the MMF will be.

The selection of fuzzy parameters should ensure that the conservative difference between the MMF and TMF is within a certain range, so as to make the establishment of the MMF reason-

able. This thesis uses loss function (LF) based on mean square error to quantify conservative differences, and confirms the level of conservatism through changes in differences, in order to maximize the feasibility of MMF. The key computational models are shown in (3.18).

$$\left\{ \begin{array}{l} \mathbf{u}_t^M = [u_{p,t}^M, u_{f,t}^M, u_{v,t}^M]^T \\ \mathbf{u}_t^T = [u_{p,t}^T, u_{f,t}^T, u_{v,t}^T]^T \\ LF = \frac{1}{T} \cdot \sum_{t=1}^T \| \mathbf{u}_t^M - \mathbf{u}_t^T \|^2 \\ \frac{dLF}{d\alpha} = \lim_{\Delta\alpha \rightarrow 0} \frac{\Delta LF}{\Delta\alpha} = \frac{LF_{i+1} - LF_i}{\alpha_{i+1} - \alpha_i} \end{array} \right. \quad (3.18)$$

Where, \mathbf{u}_t^M and \mathbf{u}_t^T are the membership vectors under the MMF and TMF, respectively. LF is the difference between membership vectors. $\frac{dLF}{d\alpha}$ calculates the degree of change of LF , i.e. slope, at different conservative levels α .

Obviously, the lower the value of α , the larger the LF value, and the higher the risk. The feasibility and conservatism of the MMF are more difficult to guarantee. Therefore, this thesis proposes a fuzzy parameter confirmation method shown as follows:

On the premise that improving TMF is more risky, try to choose a higher level of conservatism to modify them. In addition, the local maximum slope means that the change in LF is most significant within its neighborhood, indicating that the conservatism level has a significant impact on the conservatism of the MMF. So this thesis chooses the first local maximum slope to confirm the fuzzy parameters and construct the MMF. The specific steps are as follows:

Step 1: Calculate the peak-valley membership degree of the load curve of the TMF based on Figures 3.2.

Step 2: Set the initial conservatism level α to 0.95.

Step 3: Calculate the peak-valley membership degree of the MMF using (3.14)-(3.17).

Step 4: Calculate the difference of membership vectors using (3.18).

Step 5: Gradually reduce the conservatism level α and repeat **Steps 2-4** until the minimum α is reached.

Step 6: Calculate the slope of the LF using (3.18).

Step 7: Build the MMF for the corresponding fuzzy parameters with the first local maximum slope. According to (3.11)-(3.13), the peak-valley membership degrees can be further calculated,

and the initial clustering center can be obtained.

3.3.2 Initial cluster centers optimization based on data density

The initial cluster centers determined above only include peaks, valleys, and flats. When the GS determines $K > 3$, it is necessary to further explore new initial cluster centers based on the distribution of the dataset. According to the characteristics of clustering algorithms, the higher the data density in the region where the clustering center is located, the more favorable it is for clustering convergence. Therefore, this thesis proposes a method based on DD to improve the initial centers. When $K > 3$, optimize the initial cluster centers as follows:

Step 1: Define the new center between peak-flat cluster centers as v_j^{p-f} , and the new center between flat-valley cluster centers as v_j^{f-v} .

Step 2: Taking the determination of v_j^{p-f} as an example, the maximum distance between the new center and the peak-flat cluster centers is defined as $d_{\max}(v_j^{p-f})$, and the minimum distance is defined as $d_{\min}(v_j^{p-f})$.

Step 3: Define the average radius γ_j using (3.19).

$$\gamma_j = \frac{\sum_{j \in \mathbf{P}} (d_{\max}(v_j^{p-f}) + d_{\min}(v_j^{p-f}))}{2 \cdot |\mathbf{P}|} \quad (3.19)$$

Where, \mathbf{P} is the load power samples between the peak-flat clustering centers.

Step 4: Calculate the density ρ_j of the region with v_j^{p-f} as the center and γ_j as the radius. Calculate the number of samples contained in the region using (3.20).

$$\begin{cases} \rho_j = \sum_{t=1}^T \varphi(\gamma_j - d(v_j^{p-f}, x_t)) \\ \varphi(y) = 1, \quad \text{if } y \geq 0 \\ \varphi(y) = 0, \quad \text{if } y < 0 \end{cases} \quad (3.20)$$

Step 5: Take v_j^{p-f} corresponding to the maximum ρ_j as the new initial cluster center. Similarly, the second or third maximum v_j^{p-f} also applies to finding more initial centers until K determined based on the GS is satisfied. v_j^{f-v} is also determined according to the above method.

3.4 Case study

To verify the effectiveness of the proposed peak-valley periods division model, this case study conducts the analysis based on historical typical daily load data of a new energy power system in China, with a time scale of 5 minutes, as shown in Figure 3.6.

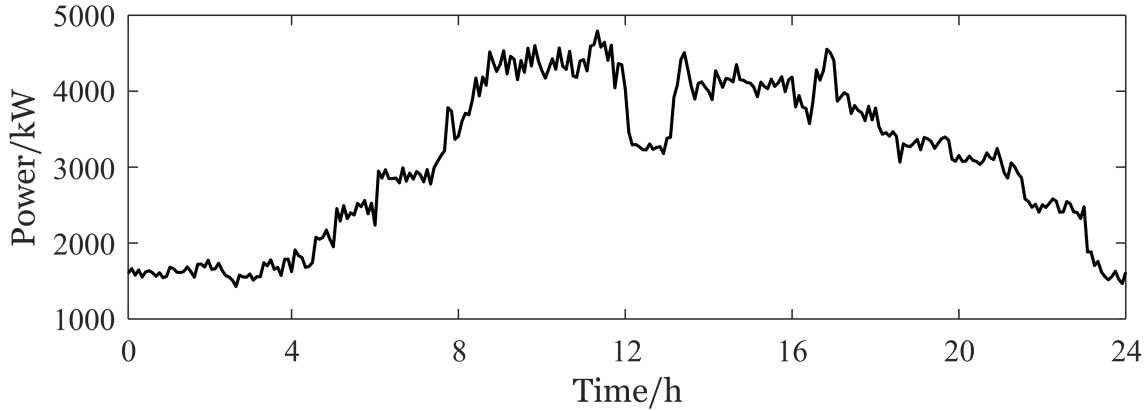


Figure 3.6: Typical daily load curve.

Firstly, according to (3.4)-(3.10), use GS to determine the optimal number of peak-valley period types K for the load curve. To ensure the accuracy of the results, the number of reference datasets B is set to 2000. The changes in statistic parameters at different k are shown in Figure 3.7.

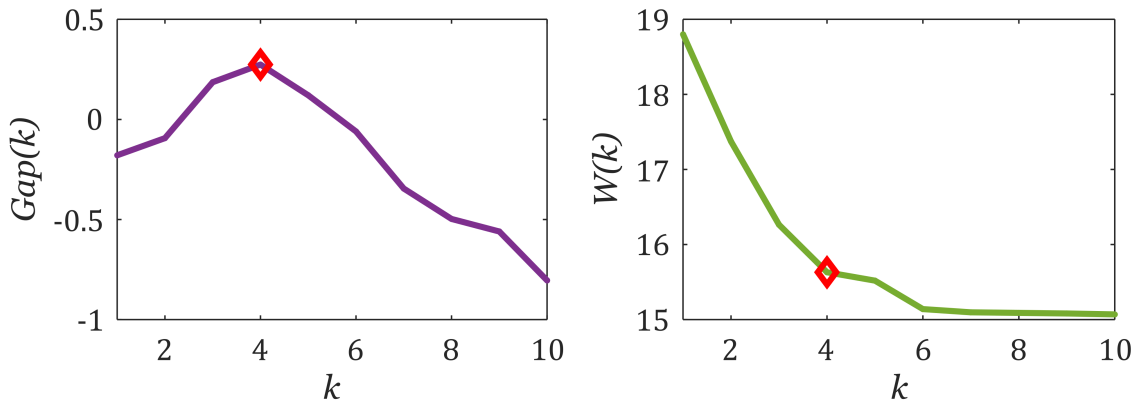


Figure 3.7: Statistic parameters under different k .

It is easy to see that the variation of $Gap(k)$ is not monotonic, showing a trend of first increasing and then decreasing. However, only when $k=4$, does it satisfy the constraint in

(3.9). $W(k)$ decreases monotonically, however, starting from $k=4$, the downward trend of $W(k)$ significantly slows down. So, the optimal number of clusters is $K=4$. This means that in addition to calculating the three cluster centers of peak, flat, and valley, it is necessary to discuss a new type of time period and calculate its initial cluster center.

Next, calculate the fuzzy parameters. According to (3.18), the relationship between the LF and the conservative level is obtained, as shown in Figure 3.8.

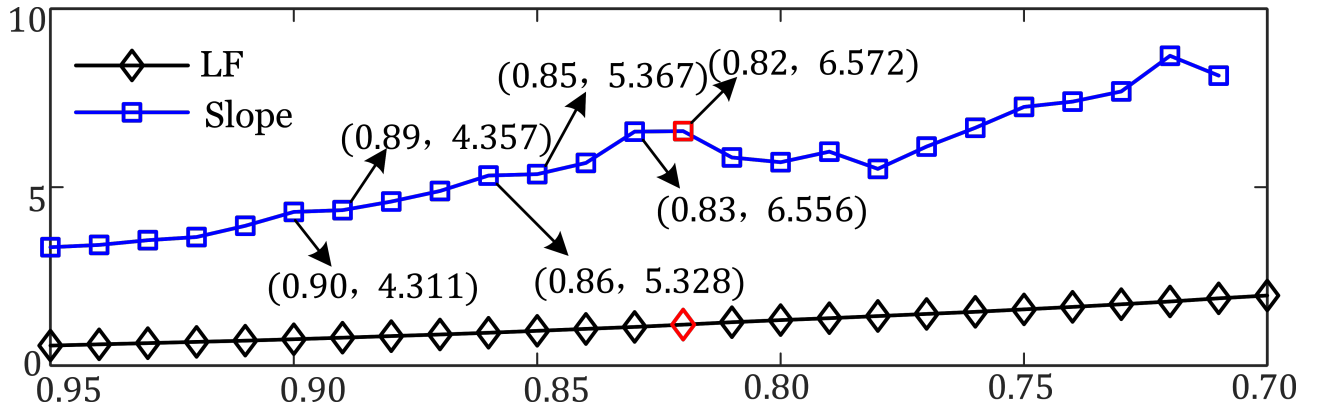


Figure 3.8: LF values and slopes at different conservative level α .

As LF value increases, the conservative level decreases, indicating a higher risk of improving the TMF. When $\alpha = 0.82$, the slope change reaches its first local maximum value, so the fuzzy parameters corresponding to this conservative level are selected. According to (3.14)-(3.17), the values of fuzzy parameters a , b , and c are shown in Table 3.1.

Table 3.1: Calculated values of fuzzy parameters a , b , c

Fuzzy parameters	Calculated values (kW)
a	2134.44
b	3110.53
c	4086.62

Build the MMF based on the parameters in Table 3.1, and obtain the peak-valley membership degree as shown in Figure 3.9. For comparison, Figure 3.10 showing the membership degrees under TMF is also given.

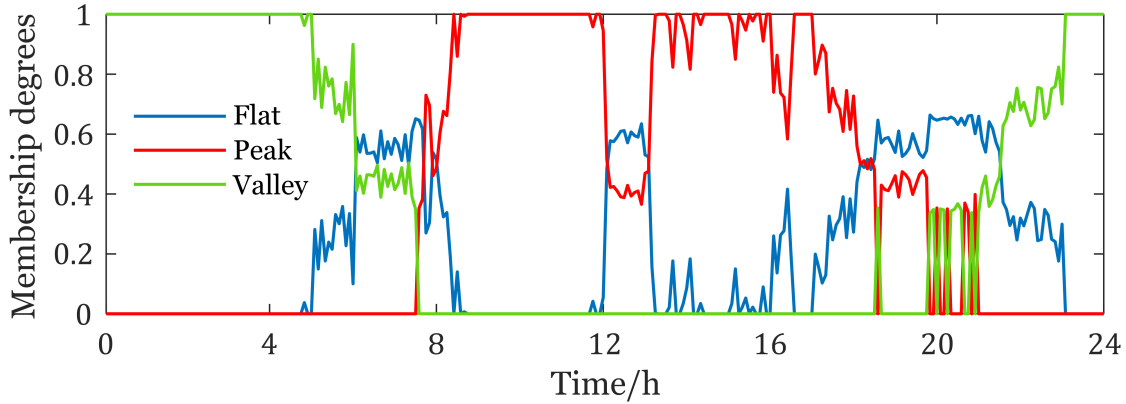


Figure 3.9: Peak-valley membership degrees under MMF.

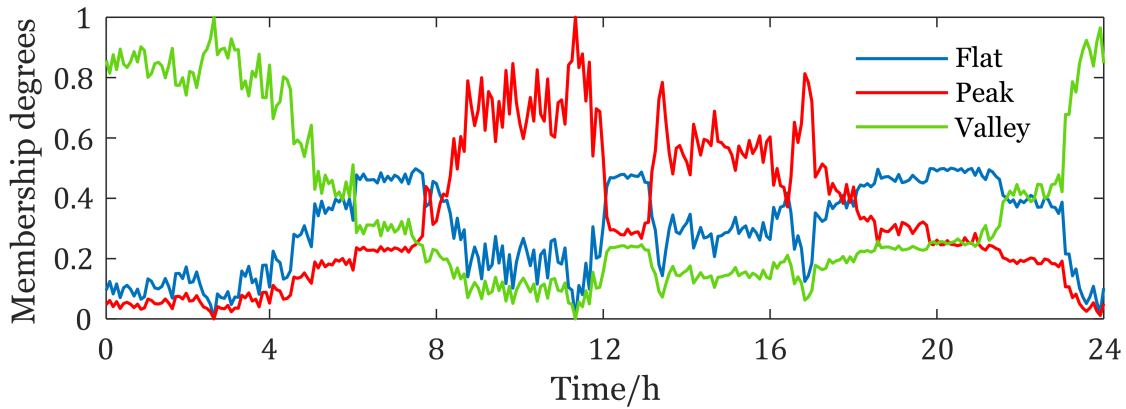


Figure 3.10: Peak-valley membership degrees under TMF.

It can be seen that the membership degrees under the MMF can maintain 0 or 1 in continuous intervals. For example: 00:00-04:00, 09:00-11:00. This judgment is clear, not vague. It is worth noting that in the early morning and late night, only two types of time periods need to be considered (flat period and valley period), which follows work and rest patterns of people. However, TMF must calculate the possibility of each time nodes belonging to three different time period types, which makes clustering initialization too conservative and results in poor computational efficiency of clustering algorithms.

Due to K=4, a new type of time period needs to be determined, so this thesis considers: the **shoulder** period between peak and flat peak periods; The **leg** period between flat and valley periods. To determine which new time period type is more in line with the characteristics of the load curve, the subsequent analysis is divided into four scenarios, as shown in Table 3.2: Scenario 1 and 2 are used to compare the clustering efficiency and results under two different

new time period types; Scenarios 3 and 4 are used to compare the impact of clustering centers initialized by MMF and TMF on clustering efficiency.

Table 3.2: Simulation scenarios

Scenarios	Clustering algorithms	Period types
Scenario 1	Improved K-Means	Peak, Shoulder , Flat, Valley
Scenario 2	Improved K-Means	Peak, Flat, Leg , Valley
Scenario 3	Improved K-Means	Peak, Flat, Valley
Scenario 4	Traditional K-Means	Peak, Flat, Valley

Table 3.3: Initial cluster centers

Period types	Initial cluster centers (kW)
Peak	3567.18
Shoulder	3124.91
Flat	2736.47
Leg	2242.57
Valley	1812.24

According to (3.11)-(3.17) and (3.19)-(3.20), the initial cluster centers for each time period are shown in Table 3.3. Then, the clustering iteration process can be obtained as shown in Figures 3.11 and 3.12.

From Figure 3.11, it can be seen that the convergence speed of scenario 2 is significantly faster, with the objective function value J already converging at the third iteration, while scenario 1 has not yet converged after 15 iterations. This indicates that for clustering using the same algorithm and the same number of clusters, different selection of initial cluster centers can significantly affect the efficiency and results of clustering.

From Figure 3.12, it can be seen that the convergence speed of scenario 3 is faster, especially after the 5th iteration. Although the objective function of all scenarios eventually converges to the same value, the significant decrease in K-Means computational efficiency caused by random initialization cannot be ignored. Overall, the initial cluster centers determined by the MMF can more effectively improve the performance of K-Means operations, while proving that MMF

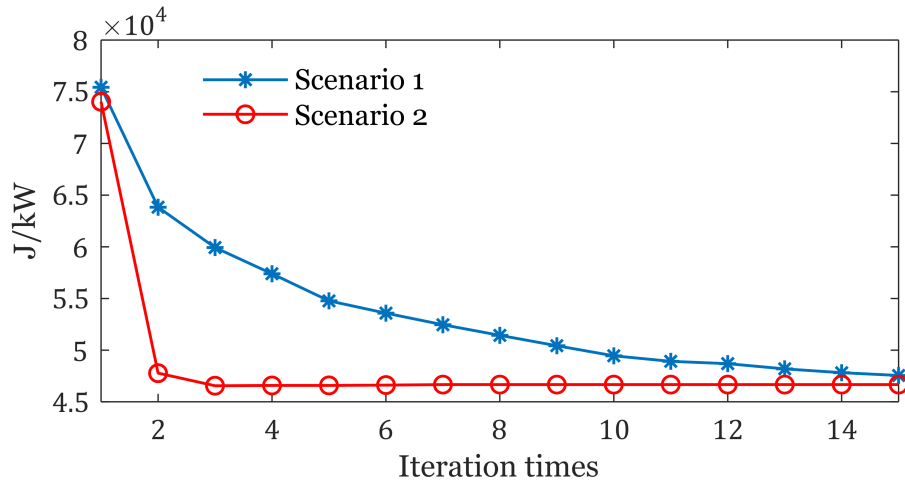


Figure 3.11: Iteration process of scenario 1 and scenario 2.

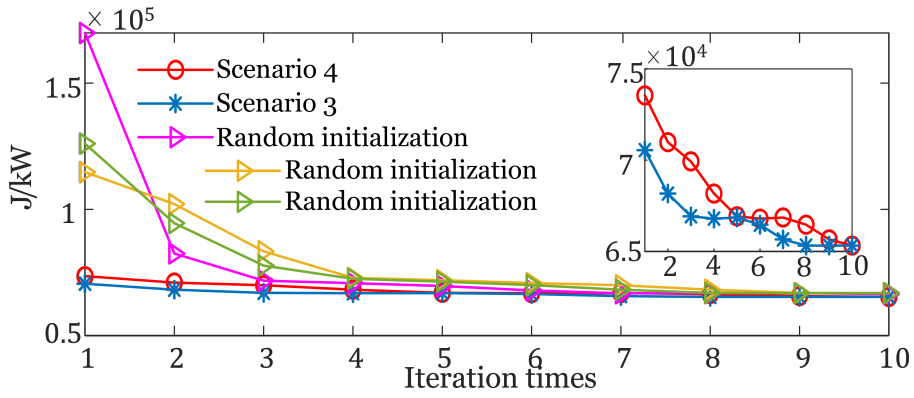


Figure 3.12: Iteration process of scenario 3 and scenario 4.

is effective in modeling the prior knowledge.

The peak-valley period division results for different scenarios are shown in Figures 3.13-3.15.

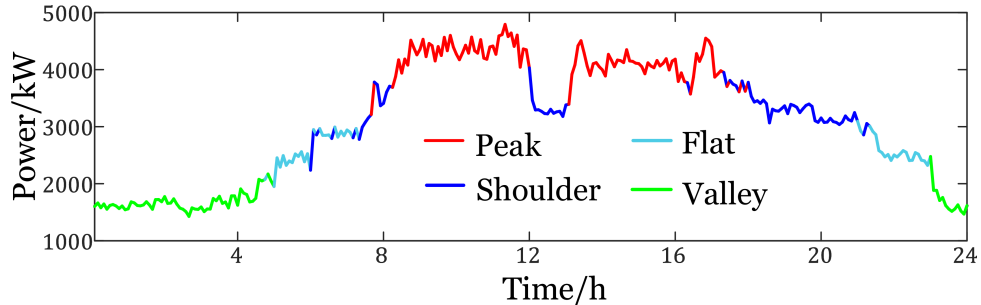


Figure 3.13: Peak-valley periods division result of scenario 1.

From the above division results, it can be seen that peak periods are mainly distributed between 08:00-12:00 and 13:00-17:00, valley periods are mainly distributed between 23:00-05:00.

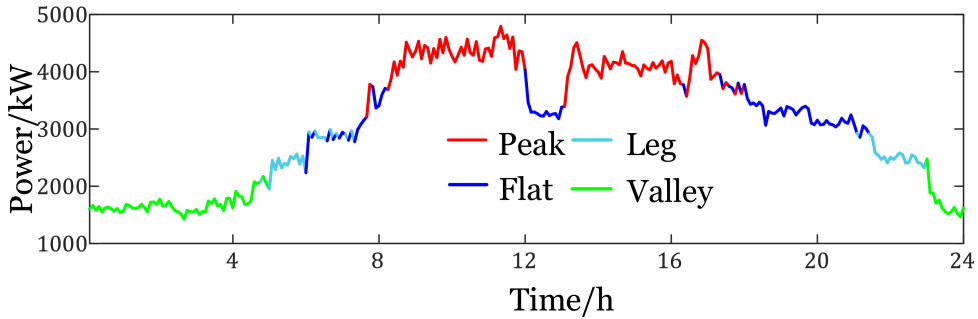


Figure 3.14: Peak-valley periods division result of scenario 2.

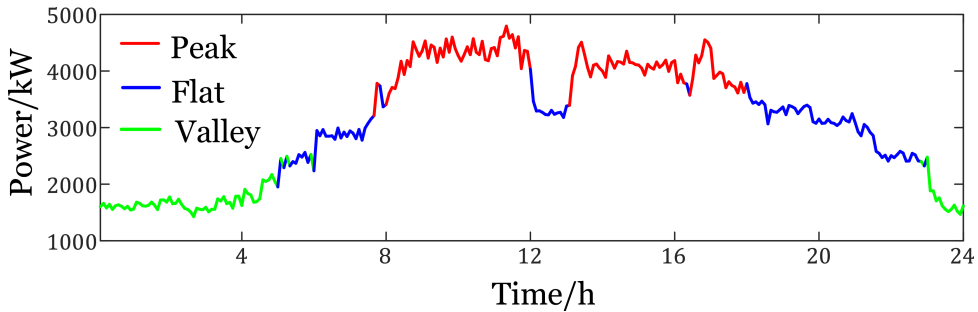


Figure 3.15: Peak-valley periods division result of scenario 3.

The distribution of other periods undergoes different changes: the changes of periods in scenarios 1 and 2 are roughly the same, but due to the new addition of shoulder and leg periods, the distributions of the flat periods in both scenarios have significant changes. This indicates that peak and valley periods have distinct numerical characteristics and can be accurately divided by K-Means, while the division of flat periods varies according to different cluster centers.

To avoid the randomness of evaluation by single indicator, this chapter uses silhouette coefficient (SC) and Davies Bouldin index (DBI) to evaluate the peak-valley period division results in different scenarios and determine the optimal period division.

The SC can reflect both the similarity of samples within clusters and the differences between samples within clusters. Therefore, it is used for evaluating the effectiveness of peak-valley periods partitioning [31]. Assuming that the average distance between sample x_i and other samples in the same cluster is $a(i)$, and the average distance between sample x_i and all samples in different clusters is $b_{k,i}$, $b(i) = \min(b_{1,i}, \dots, b_{k,i})$. The calculation of the SC is shown in 3.21.

$$SC = \frac{\sum_{i=1}^n \frac{b(i)-a(i)}{\max(a(i), b(i))}}{n} \quad (3.21)$$

Where, the larger the SC, the better the clustering effect.

The DBI is defined by Davis and Bouldin [30], and its calculation is shown in 3.22.

$$\left\{ \begin{array}{l} DBI(K) = \frac{\sum_{j=1}^K \max_{j,j \neq i} \frac{S_i + S_j}{d_{ij}}}{K} \\ S_i = \frac{1}{|c_i|} \cdot \sum_{x_t \in c_i} |x_t - z_i| \\ d_{ij} = |z_i - z_j| \end{array} \right. \quad (3.22)$$

Where, z_j is the average value of cluster c_j . d_{ij} measures the dispersion between cluster c_i and cluster c_j . The smaller the value of $DBI(K)$, the better the clustering effect.

Based on the above indicators and their properties, the evaluation results can be obtained as shown in Table 3.4.

Table 3.4: Evaluation of clustering quality

	SC	DBI
Scenario 1	0.7184	0.0064
Scenario 2	0.7069	0.0076
Scenario 3	0.7061	0.0077

According to the properties of SC and DBI, as well as the evaluation results in Table 3.4, it can be seen that the peak-valley periods division effect of scenario 1 is the best, followed by scenario 2, and finally scenario 3. Therefore, the load curve is divided into four periods: peak, shoulder, flat, valley.

3.5 Chapter conclusion

This chapter proposes an improved K-Means clustering algorithm to partition time-of-use electricity pricing periods. Compared with traditional membership functions, the initial clustering center based on modified membership functions can not only stabilize the clustering process and effect, but also further improve the computational performance of K-Means. Using gap

statistics to determine the optimal number of period types, it is found that the initial clustering centers determined by the modified membership functions do not meet the requirements. Therefore, a new initial clustering center is selected based on the density of the power data region to complete initialization and then divide the peak-valley periods. The new clustering center means a new type of load period and different division results. The silhouette coefficient and Davies Bouldin index are used to evaluate and compare different clustering results, then the load period types in this thesis are determined to be peak, shoulder, flat, valley.

Chapter 4

Abnormal Periods Correction Based on Fuzzy Subsethood

4.1 Introduction

Reasonable and effective division of peak-valley periods is a prerequisite for implementing time-of-use electricity pricing. User participation in demand response requires sufficient time to arrange electricity plans and control the operating status of loads. Therefore, the duration of each time period should be maintained at a certain length. However, from the initial peak-valley periods division (Figure 3.13), it can be seen that the load curve with a time scale of 5 minutes has the problem of frequent changes in peak-valley period types in a short time, which is not conducive to the formulation of actual scheduling plans, and users cannot make timely responses, resulting in poor time-of-use electricity pricing effects.

This chapter first elaborates on the concept of abnormal periods (APs) with rapid changes in this type of time period, and proposes corresponding correction strategies based on their distribution structure. Subsequently, establish a recognition model to identify the APs that need to be corrected. Finally, establish a correction model to convert all APs into normal periods (NPs), so that the peak-valley periods division can be used for subsequent electricity price optimization.

4.2 Definition of abnormal periods and formulation of correction strategies

Before correcting the APs, first describe its concept and structure. This chapter presents a typical distribution of APs, as shown in Figure 4.1.

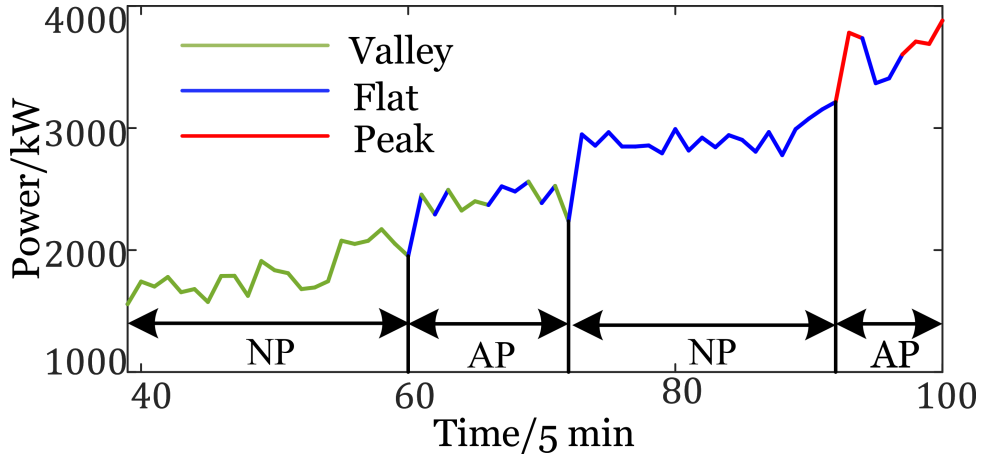


Figure 4.1: Typical structures of APs and NPs.

It can be seen that in a short time, the valley-flat periods in the first AP undergoes multiple changes; The peak-flat periods in the second AP also undergoes rapid changes, with a minimum change time of 5 minutes. This change does not allow users to arrange reasonable electricity plans, resulting in poor electricity satisfaction and ineffective peak shaving and valley filling. However, the period types in NP have not changed: the first NP is always in valley; The second NP is always in flat. Based on this characteristic, the schematic diagram of the distribution of APs can be obtained as shown in Figure 4.2.

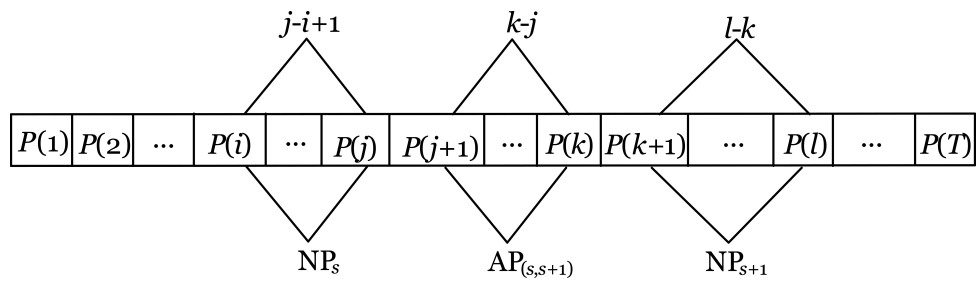


Figure 4.2: Distribution characteristics of APs.

In Figure 4.2, $P(T)$ is the power value at time point T on the load curve. $AP_{(s,s+1)}$ is

distributed between NP_s and NP_{s+1} . The durations of the first NP and the second NP are $j - i + 1$ and $l - k$, respectively, and there is only one type of period within them. The interval length of the AP is $k - j$, which contains at least two types of periods that change too quickly and come from adjacent NPs.

In order to ensure that the correction results of APs meet local characteristics, this chapter sets each AP and its adjacent NPs as a separate correction unit, and then corrects each AP one by one. Therefore, the constraint as shown in (4.1) must be satisfied.

$$\text{AP}_{(s,s+1)} \in \text{NP}_w, \quad w = \{s, s + 1\} \quad (4.1)$$

Where, $\text{AP}_{(s,s+1)}$ must have the same period type as NP_s or NP_{s+1} . Constraint (4.1) can effectively ensure the maximum continuity of time periods, preventing valley periods from being corrected to peak periods or peak periods from being corrected to valley periods.

Based on the above analysis, correct the APs in the initial periods division of scenario 1 in Chapter 3, and the correction strategy is shown in Table 4.1.

Table 4.1: Correction strategies for APs

Correction strategies	Period types of adjacent NPs	Correction for APs
Strategy 1	$\text{NP}_s = \text{NP}_{s+1}$	Classified as any NP type
Strategy 2	$\text{NP}_s = \text{Peak}, \text{NP}_{s+1} = \text{Shoulder}$	
Strategy 3	$\text{NP}_s = \text{Shoulder}, \text{NP}_{s+1} = \text{Peak}$	
Strategy 4	$\text{NP}_s = \text{Shoulder}, \text{NP}_{s+1} = \text{Flat}$	By the correction model,
Strategy 5	$\text{NP}_s = \text{Flat}, \text{NP}_{s+1} = \text{Shoulder}$	AP can be classified into
Strategy 6	$\text{NP}_s = \text{Flat}, \text{NP}_{s+1} = \text{Valley}$	period types of NP_s or NP_{s+1}
Strategy 7	$\text{NP}_s = \text{Valley}, \text{NP}_{s+1} = \text{Flat}$	

4.3 Identification model for abnormal periods

According to the analysis above, APs are distributed between different NPs. Due to the complex period types within APs, it is difficult to establish a universal identification model to directly find all different APs. However, NPs are only one of the four types: peak, shoulder flat, valley. Therefore, it is feasible to determine the location of APs by searching for NPs. Next, define the following symbols to describe the identification model:

$$\mathbf{X} = [v_1, v_2, \dots, f_i, s_{i+1}, \dots, p_j, \dots, v_T] \quad (4.2)$$

Where, v represents the valley period; f represents the flat period; s represents the shoulder period; p represents the peak period.

If \mathbf{X} has n subsequences and T numbers, they are represented as $\mathbf{X}_{s1}, \mathbf{X}_{s2} \dots \mathbf{X}_{sn}$ and $x_1, x_2 \dots x_T$, respectively. $\text{Len}\{\cdot\}$ represents the length of the sequence. $\text{First}\{\cdot\}$ Represents the first element of a sequence. The process of the identification model is shown in Table 4.2.

Table 4.2: Process of abnormal periods identification model

Algorithm 1: Abnormal periods identification model

Input: initial periods division including APs

Output: specific locations of all APs

- 1: Set the time length threshold η for NPs, create a subsequence \mathbf{X}_{sj} , confirm the first element $\text{First}\{\mathbf{X}_{sj}\}$
 - 2: **for** each element in \mathbf{X} **do**
 - 3: **if** the element is consistent with $\text{First}\{\mathbf{X}_{sj}\}$ **do**
 - 4: store the element in \mathbf{X}_{sj}
 - 5: **else if** the element is inconsistent with $\text{First}\{\mathbf{X}_{sj}\}$ **do**
 - 6: create a new subsequence and repeat the above steps
 - 7: **end if**
 - 8: **end for**
 - 9: **for** each subsequence \mathbf{X}_{sj} **do**
 - 10: **if** $\text{Len}\{\mathbf{X}_{sj}\}$ is less than η **do**
 - 11: \mathbf{X}_{sj} is an AP
 - 12: **else if** $\text{Len}\{\mathbf{X}_{sj}\}$ is larger than η **do**
 - 13: \mathbf{X}_{sj} is a NP
 - 14: **end if**
 - 15: **end for**
-

4.4 Correction model for abnormal periods

Based on the distribution characteristics of APs and corresponding correction strategies, it is necessary to consider the distribution of load data to design a correction model to determine the optimal period type of AP. Therefore, this chapter proposes a correction model based on fuzzy subsethood (FSS).

FSS represents the degree to which a fuzzy set is a subset of another fuzzy set [32]. For example, for two fuzzy sets A and B, the fuzzy subset degree of A to B can be expressed as $S(A, B)$, calculated according to (4.3).

$$S(A, B) = \frac{1}{n} \cdot \sum_{i=1}^n \frac{u_{A \cap B}(x_i)}{u_A(x_i)} = \frac{1}{n} \cdot \sum_{i=1}^n \frac{\min\{u_A(x_i), u_B(x_i)\}}{u_A(x_i)} \quad (4.3)$$

Where, $S(A, B) \in [0, 1]$, $u_A(x_i)$, and $u_B(x_i)$ are the membership degrees of x_i to fuzzy sets A and B, respectively. Here, two situations in this thesis are presented:

SIT 1: $S(A, B) = 1$ and $S(B, A) = 0$. Obviously, $A \in B$ and B cannot be a subset of A.

SIT 2: $0 < S(A, B) < S(B, A) \leq 1$. There is no clear affiliation between A and B, but the values indicate that B is more of a subset of A, represented as $B \in A$ in this thesis.

The above two situations are conducive to the correction of APs: correcting $AP_{\{s, s+1\}}$ to the period type of NP_s or NP_{s+1} is equivalent to comparing the FSS of AP belonging to two NPs, and each AP has two possible correction results, which helps to construct the model. Based on the above analysis, the correction model is as follows.

Firstly, calculate $S(u_s^{NP}, u_{s+1}^{NP})$ and $S(u_{s+1}^{NP}, u_s^{NP})$ as shown in (4.4).

$$\begin{cases} u_s^{NP} = f_s[AP_{\{s, s+1\}}] \\ u_{s+1}^{NP} = f_{s+1}[AP_{\{s, s+1\}}] \end{cases} \quad (4.4)$$

Where, u_s^{NP} is the membership degree of the power in $AP_{\{s, s+1\}}$ mapped according to f_s .

Since only two different FSS need to be considered, the membership function f_s can be

represented by (4.5).

$$f_s = \begin{cases} \varpi, & P(t) < \varsigma \\ \frac{P(t)-\varsigma-\varpi.(2.P(t)-\varsigma-\zeta)}{\zeta-\varsigma}, & \varsigma \leq P(t) < \zeta \\ 1 - \varpi, & P(t) \geq \zeta \end{cases} \quad (4.5)$$

Where, $P(t) \in AP_{\{s,s+1\}}$. ϖ is the function switch parameter. $f_{s+1} = 1 - f_s$. In strategies 2, 4, and 6, the level of NP_s is higher than NP_{s+1} , so set $\varpi = 0$, f_s is the larger membership function; For strategies 3, 5, and 7, the level of NP_s is lower than NP_{s+1} , so set $\varpi = 1$, f_s is the smaller membership function.

The different power values within the AP require f_s to choose different fuzzy parameters (ζ and ς). ζ and ς should be as close as possible to the convergence cluster centers within the NP to reflect the power characteristics. Therefore, based on the theory of FSS, select their values between NP_s and NP_{s+1} . ζ and ς are calculated by (4.6) and (4.7), respectively.

$$\left\{ \begin{array}{l} \text{Strategy 2} \Rightarrow \varpi = 0, \min|\zeta - v^p|, \min|\zeta - v^s| \\ \text{Strategy 4} \Rightarrow \varpi = 0, \min|\zeta - v^s|, \min|\zeta - v^f| \\ \text{Strategy 6} \Rightarrow \varpi = 0, \min|\zeta - v^f|, \min|\zeta - v^v| \end{array} \right\} \text{s.t. } \zeta \in NP_s, \varsigma \in NP_{s+1} \quad (4.6)$$

Where, for strategy 2, strategy 4, and strategy 6, set $\varpi = 0$. ζ and ς are selected from NP_s and NP_{s+1} respectively. v^p , v^s , v^f and v^v are the cluster centers for peak, shoulder, flat, and valley, respectively.

$$\left\{ \begin{array}{l} \text{Strategy 3} \Rightarrow \varpi = 1, \min|\varsigma - v^s|, \min|\zeta - v^p| \\ \text{Strategy 5} \Rightarrow \varpi = 1, \min|\varsigma - v^f|, \min|\zeta - v^s| \\ \text{Strategy 7} \Rightarrow \varpi = 1, \min|\varsigma - v^v|, \min|\zeta - v^f| \end{array} \right\} \text{s.t. } \varsigma \in NP_s, \zeta \in NP_{s+1} \quad (4.7)$$

Where, for strategy 3, strategy 5, and strategy 7, set $\varpi = 1$. ζ and ς are selected from NP_{s+1} and NP_s respectively.

The essence of the correction model is still to calculate the fuzzy membership degrees. What is particularly special is that according to the changes in the correction unit, namely the

changes in AP and adjacent NPs, the fuzzy parameters of the membership function need to be adjusted accordingly to characterize the local characteristics of different load data. The process of correction model is shown in Table 4.3.

Table 4.3: Process of abnormal periods correction model

Algorithm 2: Abnormal periods correction model

Input: initial periods division with APs included

Output: final periods division without APs

```

1: for each  $AP_{\{s,s+1\}}$  do
2:   if  $AP_{\{s,s+1\}}$  is consistent with correction strategy 1 do
3:      $NP_w \leftarrow AP_{\{s,s+1\}}$ 
4:   else if  $AP_{\{s,s+1\}}$  is consistent with strategies 2,4,6 do
5:     calculate  $\zeta$  and  $\varsigma$  using (4.6), then set  $\varpi = 0$ 
6:   else if  $AP_{\{s,s+1\}}$  is consistent with strategies 3,5,7 do
7:     calculate  $\zeta$  and  $\varsigma$  using (4.7), then set  $\varpi = 1$ 
8:   end if
9: end for
10: Use (4.4) and (4.5) to calculate  $S(u_s^{NP}, u_{s+1}^{NP})$  and  $S(u_{s+1}^{NP}, u_s^{NP})$ 
11: if  $S(u_s^{NP}, u_{s+1}^{NP}) > S(u_{s+1}^{NP}, u_s^{NP})$  do
12:    $NP_{s+1} \leftarrow AP_{\{s,s+1\}}$ 
13: else if  $S(u_s^{NP}, u_{s+1}^{NP}) < S(u_{s+1}^{NP}, u_s^{NP})$  do
14:    $NP_s \leftarrow AP_{\{s,s+1\}}$ 
15: end if
```

Determine the location of APs in the initial periods division of scenario 1 based on the established identification model. Subsequently, the correction model based on FSS is used to enable the initial periods division to be feasible for subsequent peak-valley electricity price optimization.

4.5 Case study

The APs in the initial periods division of scenario 1 is roughly distributed between 06:00-08:20 and 16:00-22:00. This chapter constructs a model based on FSS to correct it, where the time length threshold η for NPs is set to 6, which is 30 minutes. The comparison of peak-valley periods division before and after the correction is shown in Figures 4.3 and 4.4.

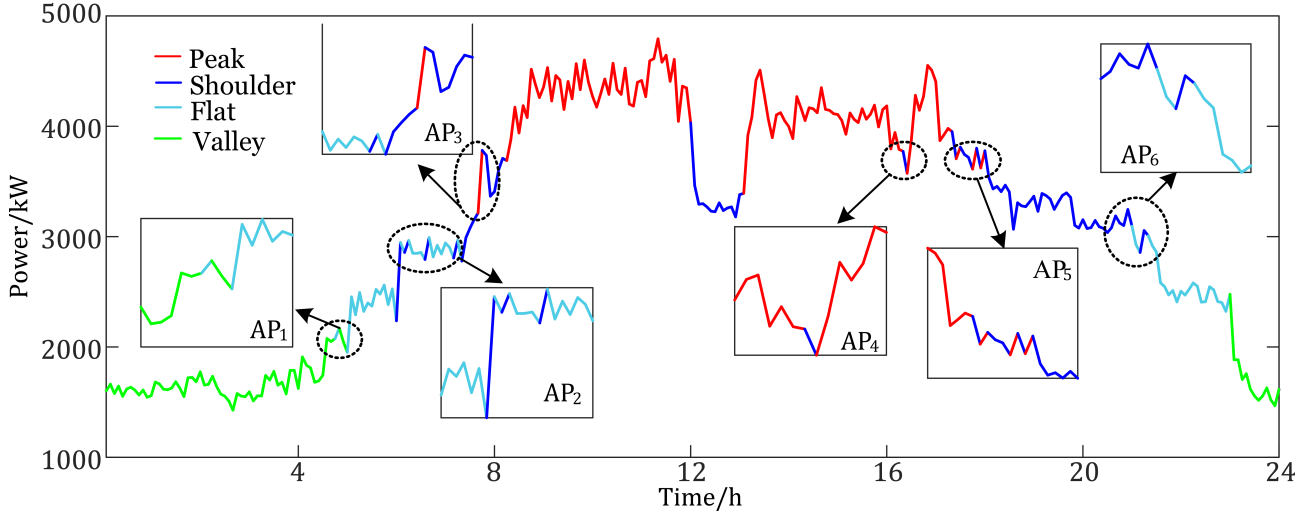


Figure 4.3: Peak-valley periods division before abnormal periods correction.

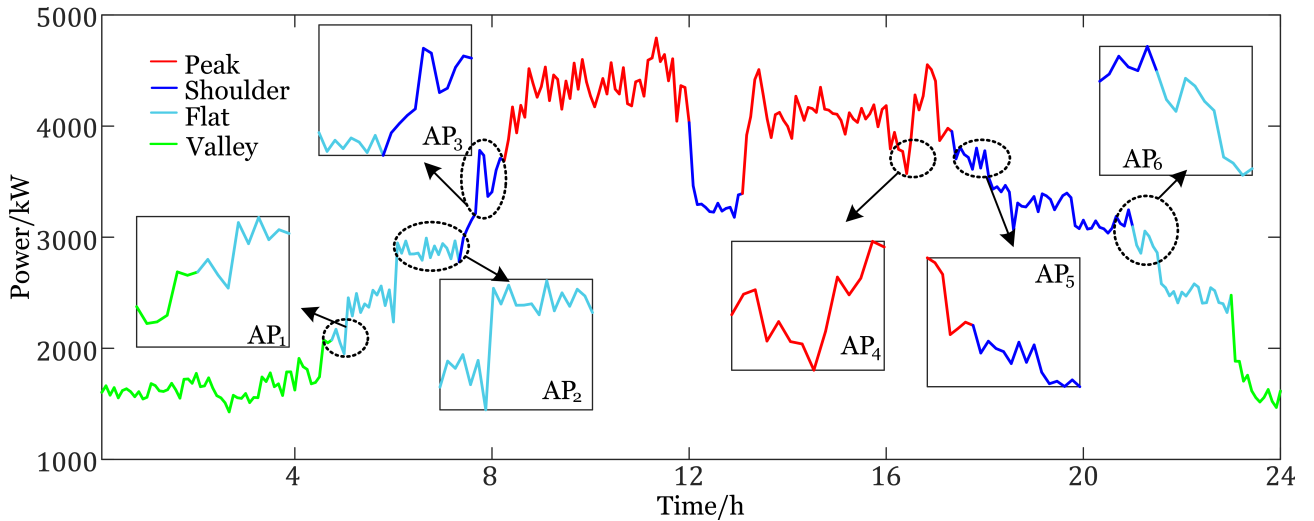


Figure 4.4: Peak-valley periods division after abnormal periods correction.

According to the comparison in Figures 4.3 and 4.4, the initial periods division of Scenario 1 has 6 APs, which include the flat-valley periods (AP₁), shoulder-flat periods (AP₂, AP₆), and peak-shoulder periods (AP₃, AP₄, AP₅). These APs are mainly distributed at the time period

type switching, and the detailed periods location are shown in Table 4.4.

Table 4.4: Specific time of different periods before and after abnormal periods correction

Period types	Initial periods division			Corrected periods division	
	NP time periods	AP time periods	Total time	NP time periods	Total time
Peak	08:15-12:00; 13:05-16:20; 16:25-17:20	07:40-07:45; 17:25-17:30; 17:45-17:50; 17:55-18:00;	8h15min	08:15-12:00; 13:05-17:20	8h
Shoulder	07:45-08:15; 12:00-13:05; 18:00-21:00	06:00-06:05; 06:10-06:15; 06:35-06:40; 07:10-07:15; 07:20-07:40; 16:20-16:25; 17:20-17:25; 17:30-17:45; 17:50-17:55; 21:10-21:20	5h55min	07:20-08:15; 12:00-13:05; 17:20-21:00;	5h40min
Flat	05:00-06:00; 06:40-07:10; 21:20-23:00	04:45-04:50; 06:05-06:10; 06:15-06:35; 07:15-07:20; 21:00-21:10	3h55min	04:45-07:20; 21:00-23:00	4h35min
Valley	00:00-04:45; 23:00-24:00	04:50-05:00	5h55min	00:00-04:45; 23:00-24:00	5h45min

According to the APs correction results, the total duration of peak period, shoulder period, and valley period decreased by 15 minutes, 15 minutes, and 10 minutes respectively, while the total duration of flat period increased by 40 minutes accordingly. Regardless of whether the APs are corrected or not, the duration ratio of peak period is the highest ($8h15min \rightarrow 8h$), followed by shoulder period ($5h55min \rightarrow 5h40min$) and valley period ($5h55min \rightarrow 5h45min$),

and finally the flat period ($3\text{h}55\text{min} \rightarrow 4\text{h}35\text{min}$). This is beneficial for users to shift more of their electricity usage time to flat periods, promoting the implementation of time-of-use policy. The types of APs before and after correction are shown in Table 4.5.

Table 4.5: Period types in abnormal periods

AP location	Initial periods division(not corrected)	Corrected periods division
AP ₁	Valley-Flat	Flat
AP ₂	Flat-Shoulder	Flat
AP ₃	Flat-Shoulder-Peak	Shoulder
AP ₄	Shoulder-Peak	Peak
AP ₅	Shoulder-Peak	Shoulder
AP ₆	Shoulder-Flat	Flat

It can be seen that the shoulder period has the highest frequency of occurrence during APs, while the valley period has the lowest frequency. This is because the power changes corresponding to shoulder periods are relatively complex, and K-Means clustering algorithm is difficult to make reasonable divisions for them, while valley periods have always been at a lower level of electricity consumption. The flat periods play a bridging role, and its increase means that the duration occupied by the previous AP is reasonably corrected.

The APs in the initial periods division include multiple types of periods, based on this variability, they are still accurately identified, reflecting the effectiveness of identifying NPs first and then determining APs. The corrected periods division mainly includes the flat periods, which is consistent with the increase in the total duration of the flat periods.

4.6 Chapter conclusion

This chapter corrects the abnormal periods in the initial periods division made by the K-Means clustering algorithm. Firstly, the structure of abnormal periods is analyzed, and their meanings are explained. Based on the above analysis, an abnormal periods correction strategy is proposed to ensure the continuity and rationality of the period type changes after correction.

Subsequently, an abnormal periods identification model is established to determine the location of the object to be corrected. Based on the principle of fuzzy subsethood, an abnormal periods correction model is established and the correction of the abnormal periods is completed.

Chapter 5

Modeling of Uncertainty in Supply and Demand Resources

5.1 Introduction

Wind and solar resources are extensively connected to the grid, and electricity consumption patterns are becoming increasingly complex. The uncertainty of supply and demand, as a factor affecting the safe and stable operation of the power system, is becoming increasingly evident. In the supply-demand relationship, the uncertainty of wind and solar resources is mainly reflected in the intermittency and volatility; The uncertainty on the demand side is mainly reflected in the electricity consumption patterns of users. With the implementation of time-of-use (ToU) electricity pricing, this uncertainty is particularly reflected in electricity transfer.

Considering the uncertainty of supply and demand can calculate the operational benefits of the system under different degrees of uncertainty, fully integrating the impact of uncertainty into the scheduling optimization results. Based on this, this chapter models the demand response (DR) and uncertainty of electricity transfer on the demand side, as well as the uncertainty of wind and solar power output on the supply side. Due to the different characteristics of elastic load and shiftable load, demand price elasticity matrix and consumer psychology are used to model them separately, and membership functions are used to simulate the uncertainty

of electricity transfer. Secondly, after determining the probability distribution of wind and solar power generation, describe the uncertain output of supply side by the budget uncertainty set.

5.2 Demand side uncertainty modeling

This chapter models the uncertainty on the demand side. Firstly, the demand price elasticity matrix is used to model the elastic load, then the shiftable load is modeled based on consumer psychology. Finally, a membership function is used to model the uncertainty of electricity transfer. In the price based DR model, nonlinear factors can be ignored [33]. The total electricity consumption Q is generated by three types of loads, as shown in (5.1).

$$Q = Q^I + Q^{II} + Q^{III} \quad (5.1)$$

Where, Q^I is generated by rigid loads, which has a weak response to electricity prices. Q^{II} is generated by elastic loads; Q^{III} is generated by shiftable loads.

5.2.1 Elastic load modeling based on demand price matrix

For elastic loads, the demand price elasticity matrix \mathbf{E} is used to characterize the response of load demand to electricity price fluctuations. The elastic coefficients in the matrix are defined according to (5.2).

$$\begin{cases} \rho_{ij} = \frac{\Delta Q^{II}(i)/Q_0^{II}(i)}{\Delta \lambda^1(j)/\lambda_0^1} \\ \Delta Q^{II}(i) = Q^{II}(i) - Q_0^{II}(i) \end{cases} \quad (5.2)$$

Where, $i, j=1, 2, 3, 4$ correspond to peak, shoulder, flat, and valley periods, respectively. ρ_{ij} is the elasticity coefficient, which represents the impact of changes in electricity price $\lambda^1(j)$ during period j on changes in electricity demand $Q^{II}(i)$ during period i . $Q_0^{II}(i)$ is the initial electricity consumption for period i . λ_0^1 is the initial electricity price for period j , which is the unified electricity price when not participating in DR. $\Delta Q^{II}(i)$ represents the change in electricity demand during period i after the implementation of the ToU policy. $\Delta \lambda^1(j)$ is the

electricity price difference during the j period after the implementation of ToU policy. Based on this, establish the DR model, as shown in (5.3) and (5.4).

$$\begin{bmatrix} \Delta Q^{\text{II}}(1)/Q_0^{\text{II}}(1) \\ \Delta Q^{\text{II}}(2)/Q_0^{\text{II}}(2) \\ \Delta Q^{\text{II}}(3)/Q_0^{\text{II}}(3) \\ \Delta Q^{\text{II}}(4)/Q_0^{\text{II}}(4) \end{bmatrix} = \mathbf{E} \cdot \begin{bmatrix} \Delta \lambda^1(1)/\lambda_0^1 \\ \Delta \lambda^1(2)/\lambda_0^1 \\ \Delta \lambda^1(3)/\lambda_0^1 \\ \Delta \lambda^1(4)/\lambda_0^1 \end{bmatrix} \quad (5.3)$$

$$\mathbf{E} = \begin{bmatrix} \rho_{11} & \rho_{12} & \rho_{13} & \rho_{14} \\ \rho_{21} & \rho_{22} & \rho_{23} & \rho_{24} \\ \rho_{31} & \rho_{32} & \rho_{33} & \rho_{34} \\ \rho_{41} & \rho_{42} & \rho_{43} & \rho_{44} \end{bmatrix} \quad (5.4)$$

Based on the above analysis, the electricity demand for each period after implementing ToU policy can be obtained, as shown in (5.5).

$$Q^{\text{II}}(i) = Q_0^{\text{II}}(i) \cdot \left(1 + \sum_{j=1}^K \rho_{ij} \cdot \frac{\Delta \lambda^1(j)}{\lambda_0^1}\right) \quad (5.5)$$

5.2.2 Shiftable load modeling based on consumer psychology

During a specific period of time of shiftable load, if the set peak-valley electricity prices increase compared to the original unified electricity price, power users often choose to transfer the electricity demand of that period to another period with cheaper electricity prices. So, the following definition is made: The period of electricity price increase is denoted as $I = \{i_1, i_2, \dots, i_m\}$, and m is the number of periods of increase; The period of electricity price decrease is denoted as $J = \{j_1, j_2, \dots, j_n\}$, and n is the number of periods of decrease. Use (5.6) to represent how the electricity transferred from period I is allocated to period J , and (5.7) to represent how the electricity absorbed from period I is allocated to period J .

$$\Delta Q^{\text{III}}(ij) = f[\Delta \lambda^1(i)].Q_0^{\text{III}}(i).|\Delta \lambda^1(j)| / \sum_{j' \in J} |\Delta \lambda^1(j')| \quad (5.6)$$

$$\Delta Q^{\text{III}}(ji) = f[|\Delta\lambda^1(j)|].Q_0^{\text{III}}(j).\Delta\lambda^1(i)/\sum_{i' \in I} |\Delta\lambda^1(i')| \quad (5.7)$$

Where, $\Delta Q^{\text{III}}(ij)$ represents the amount of electricity consumed during the transition from time period i to time period j . $\Delta Q^{\text{III}}(ji)$ represents the amount of electricity absorbed from time period i during time period j . The load transfer rate function $f(\cdot)$ is based on consumer psychology modeling, and divides the load transfer rate into three regions based on DR: dead zone, linear zone, and saturation zone. As shown in Figure 5.1.

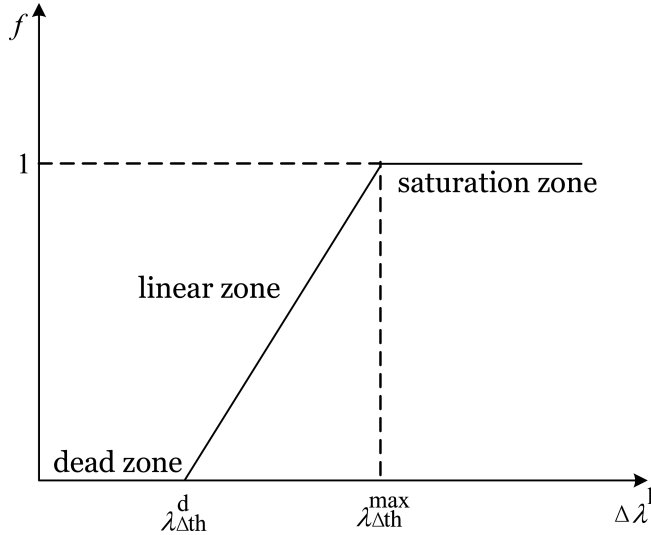


Figure 5.1: Diagram of load transfer rate function.

When the electricity price difference is small, users will not transfer electricity, so the dead zone is defined as a load transfer rate equal to 0. As the price difference increases, the possibility of users transferring electricity also increases, so the load transfer rate in the linear region is described as monotonically increasing. However, when the electricity price difference exceeds the DR threshold, the response behavior of power users no longer significantly increases with the further increase of the electricity price difference, so the load transfer rate in the saturation zone is set to the maximum value of 1. The calculation method is shown in 5.8.

$$f(|\Delta\lambda^1|) = \begin{cases} 0, & |\Delta\lambda^1| \in [0, \lambda_{\Delta\text{th}}^d) \\ \kappa.(|\Delta\lambda^1| - \lambda_{\Delta\text{th}}^d), & |\Delta\lambda^1| \in [\lambda_{\Delta\text{th}}^d, \lambda_{\Delta\text{th}}^{\text{max}}) \\ 1, & |\Delta\lambda^1| \in [\lambda_{\Delta\text{th}}^{\text{max}}, \infty) \end{cases} \quad (5.8)$$

$\lambda_{\Delta\text{th}}^{\text{max}} = 1/\kappa + \lambda_{\Delta\text{th}}^d$

Where, $|\Delta\lambda^1|$ is the absolute value of electricity price change, CNY/kW.h. $\lambda_{\Delta\text{th}}^d$ is the dead zone threshold, CNY/kW.h. $\lambda_{\Delta\text{th}}^{\max}$ is the inflection point of the saturation zone, CNY/kW.h. κ is the slope of the transition rate curve in linear zone.

Based on the electricity price of each time period, the load transfer allocation for each time period is calculated, and the DR of the shiftable load is obtained. When the set electricity price is higher than the original unified electricity price, (5.9) is used to calculate the electricity consumption level after the electricity consumption is transferred out; When the set electricity price is lower than the original unified electricity price, (5.10) is used to calculate the electricity consumption level after absorbing the transferring electricity.

$$Q^{\text{III}}(i) = Q_0^{\text{III}}(i) - \Delta Q^{\text{III}}(ij) \quad (5.9)$$

$$Q^{\text{III}}(j) = Q_0^{\text{III}}(j) + \Delta Q^{\text{III}}(ji) \quad (5.10)$$

5.2.3 Modeling of uncertainty in electricity transfer based on membership function

According to the difference in electricity prices after implementing ToU policy, there will be a clear transfer of electricity consumption of elastic loads and shiftable loads. In fact, due to various reasons, including social factors such as holidays, natural factors such as temperature and weather changes, and natural disasters, there is a certain degree of uncertainty in the transfer of electricity consumption in different periods. This chapter uses a fuzzy membership function to express this uncertainty, as shown in (5.11).

$$\mu(\Delta Q) = \begin{cases} \frac{\Delta Q - Q_{\text{th1}}}{Q_{\text{th2}} - Q_{\text{th1}}}, & Q_{\text{th1}} \leq \Delta Q < Q_{\text{th2}} \\ \frac{Q_{\text{th3}} - \Delta Q}{Q_{\text{th3}} - Q_{\text{th2}}}, & Q_{\text{th2}} \leq \Delta Q < Q_{\text{th3}} \\ 1, & \Delta Q \geq Q_{\text{th3}} \quad \text{or} \quad \Delta Q < Q_{\text{th1}} \end{cases} \quad (5.11)$$

Where, $\Delta Q = \Delta Q^{\text{II}} + \Delta Q^{\text{III}}$ is the quantity of DR. Q_{th1} , Q_{th2} and Q_{th3} are function parameters determined by response quantities. The transfer electricity consumption Q_{th2} is given in advance

in a deterministic environment, and the calculation of other parameters is shown in (5.12).

$$\begin{cases} Q_{\text{th}1} = (1 - \gamma).Q_{\text{th}2} \\ Q_{\text{th}3} = (1 + \gamma).Q_{\text{th}2} \end{cases} \quad (5.12)$$

Where, $\gamma \in [0, 1]$ represents the degree of uncertainty in electricity transfer. The smaller the value of γ , the smaller the uncertainty interval, and the users have a clearer plan for electricity transfer; The larger the value of γ , the greater the uncertainty of electricity transfer. When the user response quantity is $\Delta Q < Q_{\text{th}1}$ or $\Delta Q \geq Q_{\text{th}3}$, it indicates that the DR to different electricity prices is clear and a clear electricity consumption plan has been arranged; When the user response quantity is $Q_{\text{th}1} \leq \Delta Q < Q_{\text{th}3}$, there is a certain degree of uncertainty in the transfer of electricity.

Based on the above, the load curve considering the uncertainty of electricity transfer can be obtained as (5.13).

$$\begin{cases} \widetilde{Q_{\text{DR}}} = Q^{\text{I}} + Q_{\text{DR}}^{\text{II}} + Q_{\text{DR}}^{\text{III}} \\ Q_{\text{DR}}^{\text{II}} + Q_{\text{DR}}^{\text{III}} = \mu(\Delta Q).(\Delta Q^{\text{II}} + \Delta Q^{\text{III}}) + Q^{\text{II}} + Q^{\text{III}} \end{cases} \quad (5.13)$$

Where, $Q_{\text{DR}}^{\text{II}}$ and $Q_{\text{DR}}^{\text{III}}$ are the uncertain electricity consumption of elastic load and shiftable load after participating in DR, respectively.

5.3 Supply side uncertainty modeling

The output uncertainty of wind turbines (WTs) and photovoltaic systems (PVs) is described using the budget uncertainty set under probability distribution. Among them, the output of WTs follows weibull distribution (WD), while the output of PVs follows beta distribution (BD).

5.3.1 Probability distribution of wind turbines output

The wind speed is a key factor determining the output of WTs. From a statistical perspective, it can be concluded that wind speed follows WD [34], and its probability density function is shown in (5.14).

$$f(v_t) = \frac{k_t}{\lambda_t} \cdot \left[\frac{v_t}{\lambda_t} \right]^{k_t-1} \cdot \exp^{-\left[\frac{v_t}{\lambda_t} \right]^{k_t}} \quad (5.14)$$

Where, v_t is the wind speed during time period t . k_t and λ_t are the shape and scale parameters, respectively.

The wind speed-probability density distribution curve is shown in Figure 5.2.

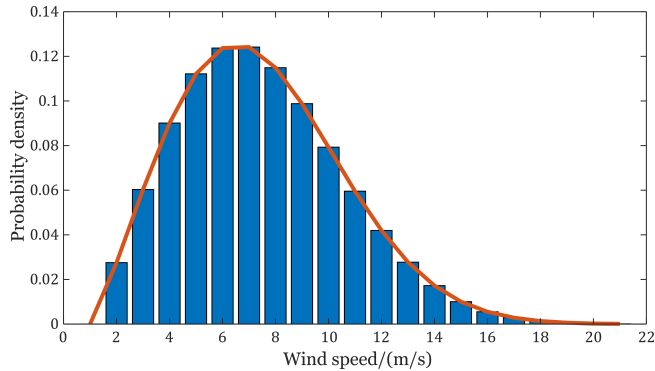


Figure 5.2: Wind speed-probability density distribution curve.

According to (2.1)), it can be seen that the output of WTs is approximately linearly related to wind speed. For the convenience of research, this thesis assumes that their output characteristics also approximately follow a WD.

5.3.2 Probability distribution of photovoltaic systems output

Ignoring other nonlinear factors, the intensity of light is the key factor determining the output of PVs. Therefore, its output characteristics are similar to those of WTs. The light intensity

generally follows a BD [35], and its probability density function is shown in (5.15).

$$\left\{ \begin{array}{l} f(Li_t) = \frac{G(v_t) + \zeta_t}{G(v_t) + G(\zeta_t)} \cdot Li_t^{(v_t-1)} \cdot (1 - Li_t)^{\zeta_t-1} \\ Li_t = \frac{P_{PV(t)}}{P_{PV,r}} \\ \mu_t = \frac{v_t}{v_t + \zeta_t} \\ \sigma_{S,t}^2 = \frac{v_t \cdot \zeta_t}{(v_t + \zeta_t)^2 \cdot (v_t + \zeta_t + 1)} \end{array} \right. \quad (5.15)$$

Where, Li_t represents the light intensity during time period t . v_t and ζ_t are shape parameters. $G(\cdot)$ is gamma function. $P_{PV}(t)$ and $P_{PV,r}$ are the output power and rated power of the PVs, respectively. μ_t and $\sigma_{S,t}^2$ are the expected value and variance of the light intensity, respectively.

The light intensity-probability density distribution curve is shown in Figure 5.3.

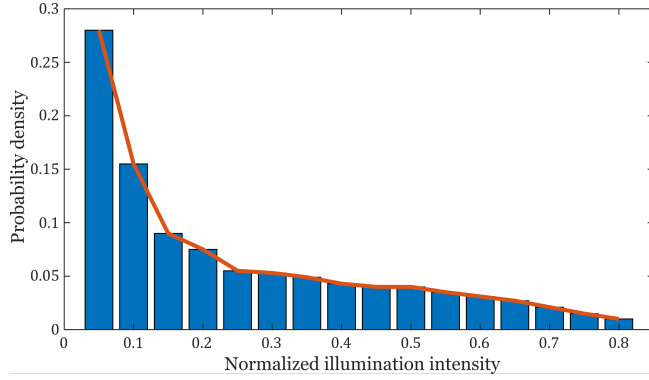


Figure 5.3: Light intensity-probability density distribution curve.

According to (2.3), the output of PVs is linearly related to the intensity of light. For the convenience of research, this thesis assumes that its output approximately follows a BD.

5.3.3 Wind and solar power output modeling based on budget uncertainty set

Robust uncertainty set is a closed nonlinear parameter model based on intervals, including simple uncertain intervals represented by box uncertainty set, which contains all possible values of the decision parameters [36]. But this uncertainty set usually cannot consider data features, resulting in overly conservative solution results. Therefore, budget uncertainty set (BUS) is

developed [37], as shown in (5.16).

$$\text{BUS} = \{\zeta : \sum | \frac{\zeta_i - \hat{\zeta}_i}{\bar{\zeta}_i - \underline{\zeta}_i} | \leq \Gamma, |\zeta| \leq \mathbf{e} \} \quad (5.16)$$

Where, ζ is the uncertainty parameter vector. $\hat{\zeta}_i$ is the expected or predicted value vector of uncertainty parameters. $\bar{\zeta}_i$ and $\underline{\zeta}_i$ are the upper and lower bounds of the parameters, respectively. Γ is the uncertainty, used to characterize the range of uncertainty parameter disturbances.

This chapter assumes that the available output of WTs and PVs belongs to the box uncertainty set, and the actual output is within the budget uncertainty set. By controlling the uncertainty, the fluctuation range of wind and solar power output can be adjusted to analyze the optimization results of scheduling under different uncertainties. The uncertainty sets of WTs and PVs are shown in (5.17).

$$\left\{ \begin{array}{l} \text{BUS}_{\text{WT}} = \{\widetilde{\mathbf{P}_{\text{WT}}} \in \{[\mathbf{P}_{\text{min}}^{\text{WT}}, \mathbf{P}_{\text{max}}^{\text{WT}}] \sim \text{WD}\} \mid \sum_{t=1}^T \left| \frac{\widetilde{P}_{\text{WT}}(t) - P_{\text{WT}}(t)}{\overline{P}_{\text{WT}}(t) - \underline{P}_{\text{WT}}(t)} \right| \leq \Gamma \cdot T\} \\ \text{BUS}_{\text{PV}} = \{\widetilde{\mathbf{P}_{\text{PV}}} \in \{[\mathbf{P}_{\text{min}}^{\text{PV}}, \mathbf{P}_{\text{max}}^{\text{PV}}] \sim \text{BD}\} \mid \sum_{t=1}^T \left| \frac{\widetilde{P}_{\text{PV}}(t) - P_{\text{PV}}(t)}{\overline{P}_{\text{PV}}(t) - \underline{P}_{\text{PV}}(t)} \right| \leq \Gamma \cdot T\} \end{array} \right. \quad (5.17)$$

Where, $\mathbf{P}_{\text{max}}^{\text{WT}}$ and $\mathbf{P}_{\text{min}}^{\text{WT}}$ are the upper and lower vectors of the available output of the WTs, which follow the WD in (5.14); $\mathbf{P}_{\text{max}}^{\text{PV}}$ and $\mathbf{P}_{\text{min}}^{\text{PV}}$ are the upper and lower vectors of the available output of the PVs, and follow the BD in (5.15).

To calculate the upper and lower vectors of (5.17), the first step is to predict the wind and solar power output during the scheduling period; Secondly, a large number of wind and solar power output scenarios that follow probability distributions are simulated using Latin hypercube sampling (LHS), and then reduced to typical output scenarios using a fast predecessor elimination method based on probability distance; Then, in multiple typical scenarios, search for the maximum and minimum values of the power sampling points at each time node: the maximum sequence of wind and solar power output is taken as $\mathbf{P}_{\text{max}}^{\text{WT}}$ and $\mathbf{P}_{\text{max}}^{\text{PV}}$, and the minimum sequence is taken as $\mathbf{P}_{\text{min}}^{\text{WT}}$ and $\mathbf{P}_{\text{min}}^{\text{PV}}$. The general process of LHS is as follows:

Step 1: Determine the number of samples to be extracted N.

Step 2: Hierarchical the input probability distribution. Divide the cumulative curve into equal

intervals on the cumulative probability scale (0-1.0). For an n-dimensional vector space, each dimension will be divided into N non overlapping intervals, so that each interval has the same probability.

Step 3: Random sampling. For each one-dimensional vector space, randomly select a sample from each interval.

Step 4: Combine samples. Randomly selected samples from each dimension are combined into a vector.

Step 5: Disrupt the sampling order. To increase the randomness of the sample, it is necessary to shuffle the sampling order.

5.4 Net load modeling based on supply and demand uncertainty resources

The net load of the power system is the difference between the actual electricity consumption and the generated electricity within the system. This difference directly reflects the power that the system needs to input or output from the outside, especially when considering the integration of clean energy (such as WTs, PVs, etc.). The definition of net load is extended to the difference between load demand and clean energy output capacity, that is, the additional power that the supply side needs to output after consuming clean energy, and this part of load demand is fulfilled by other power generation units.

In this thesis, the output of gas turbines and battery energy storage systems is used to meet net load demands, as shown in (5.18).

$$\widetilde{P_{NL}(t)} = \widetilde{P_{DR}(t)} - \widetilde{P_{PV}(t)} - \widetilde{P_{WT}(t)} \quad (5.18)$$

Where, $\widetilde{P_{NL}(t)}$ is the net load at time period t . $\widetilde{P_{DR}(t)}$ is the power value after DR.

5.5 Chapter conclusion

This chapter models the uncertainty of supply and demand. Firstly, the demand price elasticity matrix and consumer psychology are used to model the elastic load and shiftable load respectively. Finally, the fuzzy membership function is used to characterize the uncertainty of electricity transfer. For the supply side, first analyze that the output of wind turbines follows a weibull distribution, and the output of photovoltaic power generation systems follows a beta distribution. Then, combined with the above probability distributions, model the uncertain output of wind and solar power based on the budget uncertainty set. Finally, in order to fully absorb the wind and solar power output, the net load is constructed based on the established supply and demand uncertainty resources.

Chapter 6

Optimization of Time-of-Use Tariff for the New Energy Power System

6.1 Introduction

The key factors in the formation of time-of-use (ToU) tariff policy are the division of peak-valley periods and reasonable pricing. After determining the peak-valley periods, this chapter considers the uncertainty of supply and demand, with the goal of achieving the best comprehensive benefits of system operation, to formulate peak-valley tariff, and deeply explore the coupling relationship between tariff, uncertainty, and economic dispatch. Firstly, explain the necessary assumptions and clarify the strategy for peak-valley tariff. Then, establish the objective function and constraints of the optimization model. Secondly, establish a solution model that combines hippopotamus optimization algorithm and CPLEX solver to transform difficult nonlinear programming problems into linear programming problems for solving. Finally, establish different simulation scenarios and analyze the coupling relationship based on the simulation results and comparisons of different scenarios.

6.2 Time-of-use tariff strategy formulation

From the perspective of pricing, the link of generation mainly focuses on the onto-grid prices of different power sources on the supply side; The link of transmission and distribution (T-D) process mainly targets the T-D prices of grid side; The link of selling electricity mainly focuses on the prices of different loads on the demand side during peak-valley periods. In addition, power grid enterprises also undertake the responsibility of collecting government funds.

From the perspective of different links, the onto-grid prices λ^s mainly compensate for the power generation cost; The T-D prices λ^g are mainly used to compensate for the operating costs of the power grid; Government funds λ^f are non tax revenues collected through electricity prices approved by the state council; The selling electricity prices λ^l are the final electricity cost that power users need to pay. They have a relationship as shown in (6.1).

$$\lambda^l = \lambda^s + \lambda^g + \lambda^f \quad (6.1)$$

Where, λ^f is difficult to confirm and can be ignored [38]. Therefore, the strict relationship of (6.1) can be relaxed into a relationship as shown in (6.2).

$$\begin{cases} \lambda^l \geq \lambda^s + \lambda^g \\ \overline{\lambda^l} = \overline{\lambda^s} + \overline{\lambda^g} \\ \underline{\lambda^l} = \underline{\lambda^s} + \underline{\lambda^g} \end{cases} \quad (6.2)$$

Where, $\overline{\lambda^l}$ and $\underline{\lambda^l}$ are the upper and lower bounds of the relaxed electricity selling prices, respectively; $\overline{\lambda^s}$ and $\underline{\lambda^s}$ are the upper and lower bounds of the relaxed onto-grid electricity prices, respectively; $\overline{\lambda^g}$ and $\underline{\lambda^g}$ are the upper and lower bounds of the relaxed T-D electricity prices, respectively.

After determining the peak-valley periods and the range of electricity prices, the optimization can be completed by calculating the electricity prices for each link based on the optimal comprehensive benefits of the system. For the convenience of research, this thesis assumes that the onto-grid electricity prices of different power sources are the same, and the electricity selling

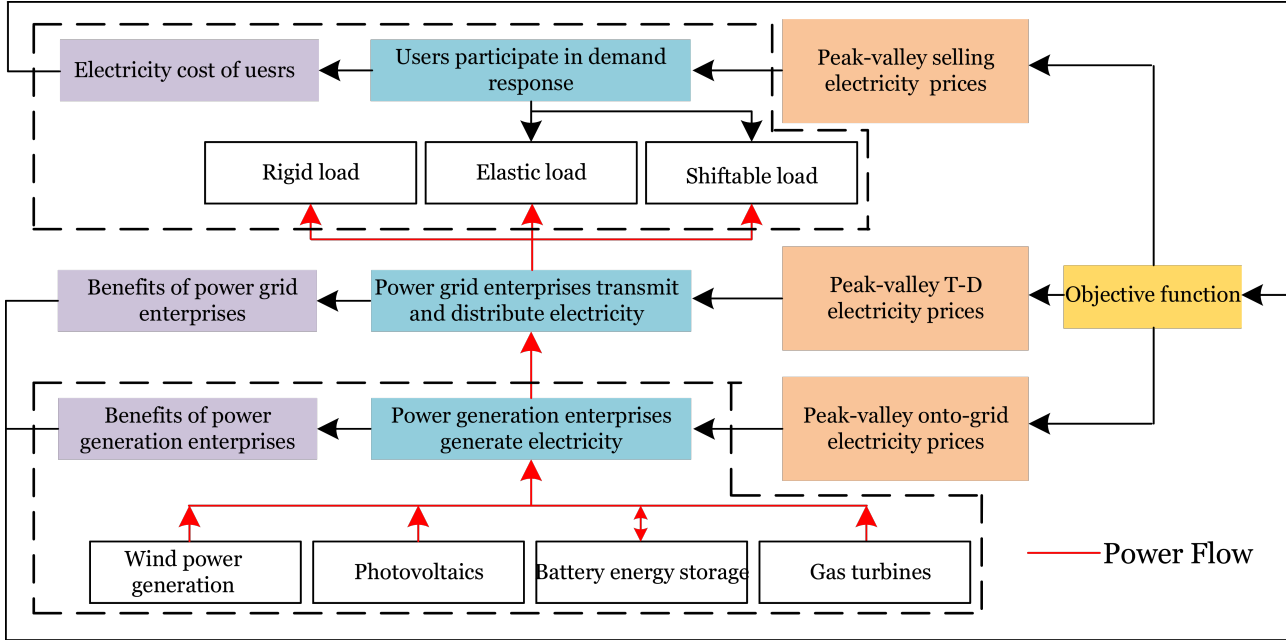


Figure 6.1: Framework for time-of-use tariff design mechanism.

prices for different power users are the same. Based on the above analysis and assumptions, the ToU tariff strategy can be obtained as shown in Figure 6.1.

As shown in Figure 6.1, after the implementation of ToU policy, different types of loads will participate in the demand response according to the difference in the selling prices, adjust the power consumption plan, and form a new power consumption curve and user power cost. According to the constraints of supply-demand balance, power generation will be arranged to output in an orderly manner, connect to the grid at the onto-grid prices, meet load demand, and obtain power generation benefits. Power grid enterprises distribute electricity to different types of loads according to load demand, while obtaining T-D profits. The generation, T-D, and usage of electricity are carried out simultaneously, and the objective function considers the comprehensive benefits of different links by optimizing and adjusting the electricity prices of different links to achieve the optimal comprehensive benefits.

6.3 Time-of-use tariff optimization model

The ToU tariff optimization model considers the cost of electricity consumption on the demand side, the T-D benefits on the grid side, and the generation profits on the supply side. It

formulates objective functions and constraints that take into account the benefits of each link, and finally uses the hippopotamus optimization algorithm and CPLEX solver to solve the optimal electricity price for each time period, so as to achieve the optimal comprehensive benefits of the system.

6.3.1 Objective function

When the benefits of the grid side and supply side are maximized, and the electricity cost of demand side is minimized, the comprehensive benefits of the system reach the optimal level, which can be expressed by (6.3).

$$\max F = \max F^s + \max F^g - \min F^l \quad (6.3)$$

Where, F^s , F^g , and F^l respectively represent the power generation benefits of supply side, T-D benefits of grid side, and electricity consumption cost of demand side after the implementation of ToU policy. The following is a specific explanation of the benefits of each link:

The electricity cost of users is mainly composed of the electricity bills generated by purchasing electricity from the grid. After implementing ToU policy and user participation in demand response, the fee they need to pay is calculated and represented by (6.4).

$$F^l = \sum_k^K \sum_{t \in T_k} \lambda^l(t) \cdot \widetilde{P_{DR}(t)} \quad (6.4)$$

Where, $\lambda^l(t)$ is the selling price at time t after implementing the ToU policy. k represents different types of time periods; K is the total number of time period types, which includes peak, shoulder, flat, valley, so K is equal to 4.

After implementing ToU policy, the benefits of power grid enterprises is represented by (6.5).

$$F^g = \sum_k^K \sum_{t \in T_k} \lambda^g(t) \cdot \widetilde{P_{DR}(t)} - C^g \quad (6.5)$$

Where, $\lambda^g(t)$ is the T-D prices after implementing ToU policy. C^g is the cost of T-D, represented by (6.6).

$$C^g = \sum_{t=1}^T \eta^g \cdot \widetilde{P_{DR}(t)} \quad (6.6)$$

Where, η^g is the cost coefficient of T-D by power grid.

After implementing time of use electricity pricing, the revenue of power generation enterprises can be represented by equation (6.7).

$$F^s = \sum_k^K \sum_{t \in T_k} \lambda^s(t) \cdot \widetilde{P_{DR}(t)} - C^s \quad (6.7)$$

Where, $\lambda^s(t)$ is the onto-grid prices after implementing ToU policy. C^s is the cost of power generation, which includes the operating costs of gas turbines, batteries, and wind and solar power units, represented by (6.8).

$$C^s = \sum_{t=1}^T C_{GT}(t) + C_{BESS}(t) + C_{WT}(t) + C_{PV}(t) \quad (6.8)$$

In summary, the objective function (6.3) can be rewritten as (6.9).

$$\left\{ \begin{array}{l} \max F = \sum_k^K \sum_{t \in T_k} (\lambda^s(t) + \lambda^g(t) - \lambda^l(t)) \cdot \widetilde{P_{DR}(t)} - C^s - C^g \\ F \propto [\lambda^s, \lambda^g, \lambda^l, P_{GT}(t), P_{BESS}^{dis}(t), P_{BESS}^{ch}(t), U_{BESS}(t), \widetilde{P_{PV}(t)}, \widetilde{P_{WT}(t)}] \end{array} \right. \quad (6.9)$$

6.3.2 Constraints

The operational constraints of the power generation units on supply side include: Gas turbines: (2.6), (2.7); Battery energy storage system: (2.9)-(2.12); Wind turbines and photovoltaic system: (5.17). In addition to the above constraints, the supply-demand balance constraint must be satisfied, as shown in (6.10).

$$P_{GT}(t) + P_{BESS}^{dis}(t) - P_{BESS}^{ch}(t) = \widetilde{P_{NL}(t)} \quad (6.10)$$

The constraints related to electricity prices and demand response at each link also need to be considered to ensure that the implementation of ToU policy can improve system economy. The following is a specific explanation of the constraints:

For power users on the demand side, the upper and lower limits of the electricity selling price for each period are represented by (6.11).

$$\lambda_{\min,k}^l \leq \lambda_k^l \leq \lambda_{\max,k}^l \quad (6.11)$$

Where, λ_k^l is the selling price for time period type k . $\lambda_{\max,k}^l$ and $\lambda_{\min,k}^l$ are the upper and lower limits of the price, respectively.

For power grid enterprises, the upper and lower limits of T-D electricity prices at different time periods are represented by (6.12).

$$\lambda_{\min,k}^g \leq \lambda_k^g \leq \lambda_{\max,k}^g \quad (6.12)$$

Where, λ_k^g is the T-D price for time period type k . $\lambda_{\max,k}^g$ and $\lambda_{\min,k}^g$ are the upper and lower limits of the price, respectively.

For power generation enterprises, the upper and lower limits of onto-grid prices at different time periods are represented by (6.13).

$$\lambda_{\min,k}^s \leq \lambda_k^s \leq \lambda_{\max,k}^s \quad (6.13)$$

Where, λ_k^s is the onto-grid price for time period type k . $\lambda_{\max,k}^s$ and $\lambda_{\min,k}^s$ are the upper and lower limits of the price, respectively.

The above prices are subject to (6.2), therefore there are constraints shown in (6.14).

$$\left\{ \begin{array}{l} \lambda_{\min,k}^l = \lambda_{\min,k}^g + \lambda_{\min,k}^s \\ \lambda_{\max,k}^l = \lambda_{\max,k}^g + \lambda_{\max,k}^s \end{array} \right. \quad (6.14)$$

Due to the fact that the ToU policy includes four periods, which can effectively widen the ratio of peak-valley prices and prevent peak-valley inversion, this thesis does not set the ratio as shown in [38]. Given that users typically prefer to consume electricity during peak hours, their electricity costs will not experience significant fluctuations and are allowed to increase within a certain range. This change constraint is represented by (6.15).

$$(1 - \omega)F_0^l \leq F^l \leq (1 + \omega)F_0^l \quad (6.15)$$

Where, ω is the fluctuation parameter of electricity cost of users. F_0^l is the cost before the implementation of ToU policy. The unified selling price, T-D price, and onto-grid price are respectively named λ_0^l , λ_0^g , and λ_0^s .

6.3.3 Solving model

According to the process of demand response, it can be concluded that the above optimization model is a mixed integer nonlinear programming. The process of solving the nonlinear part mainly involves two parts: the product of electricity prices and power in each link, the product of selling prices and power. Therefore, using only CPLEX for solving requires extremely complex formula derivation and program writing, and it is difficult to ensure a complete demand response process. Based on the above considerations, this thesis proposes a solving model that combines hippopotamus optimization algorithm (HOA) with CPLEX solver to transform the original problem into a linear programming problem.

The HOA is conceived inspired by the inherent behavior of hippopotamus [39]. It is based on population optimization and consists of two stages: exploration and exploitation. Among them, the position of each hippopotamus in the search space is represented by a vector, which is the value of the decision variable. The specific process of the algorithm will not be elaborated here. The solving model based on HOA-CPLEX is shown in Figure 6.2.

The model consists of two layers: the outer layer is the HOA, which is used to generate the optimal solutions for peak-valley electricity prices for demand side/users, grid side/grid

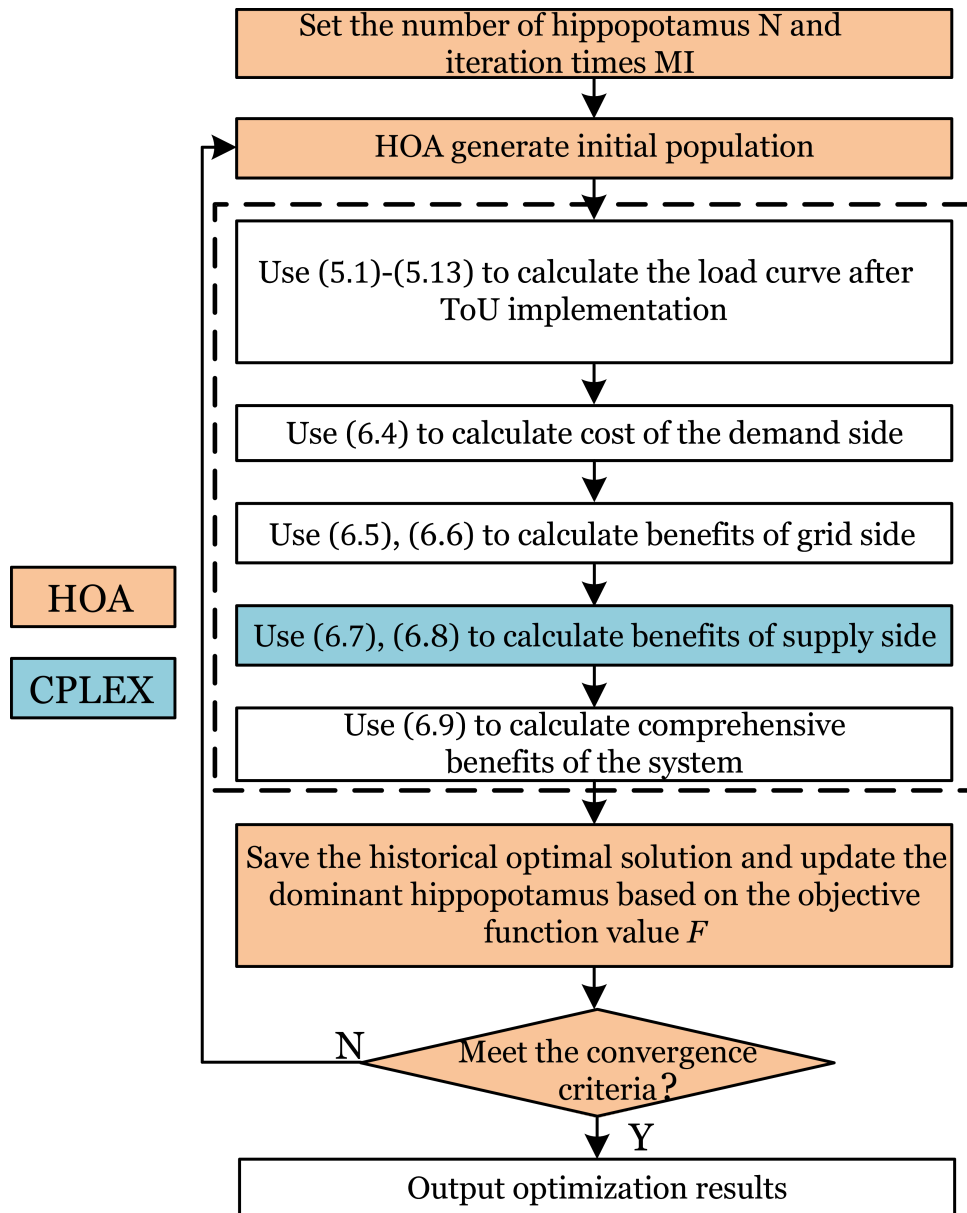


Figure 6.2: Solving model based on the hippopotamus optimization algorithm and CPLEX.

enterprises, and supply side/power generation enterprises, and pass them to the inner layer. Then, the values of the solutions are adjusted based on the returned objective function values. The inner layer is CPLEX, which is used to calculate the optimal objective function value based on the electricity prices from HOA and return this value to the outer layer.

6.4 Case study

6.4.1 Simulation settings and instructions

Before conducting the case study, it is necessary to provide explanations for the key parameter settings. Firstly, the available output ranges of wind turbines (WTs) and photovoltaic systems (PVs) are provided. The ranges of the two are based on weibull probability distribution, beta distribution, and latin hypercube sampling, as shown in Figures 6.3 and 6.4, respectively.

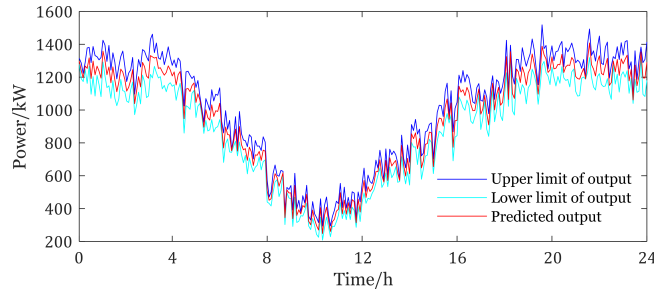


Figure 6.3: Output range of wind turbines.

It can be seen that the output time of the PVs is between 04:30-18:00. The output of the WTs is lower between 08:00-12:00, while the output of the PVs is higher. The two outputs form complementarity, but have obvious fluctuations. In addition to the output range of WTs and PVs, parameters related to the operation of power generation units, demand response, and constraints on electricity prices in each link need to be provided, as shown in Table 6.1. To fully analyze the impact of supply-demand uncertainty and ToU tariff on economics of the system operation, the case study is divided into four scenarios, as shown in Table 6.2.

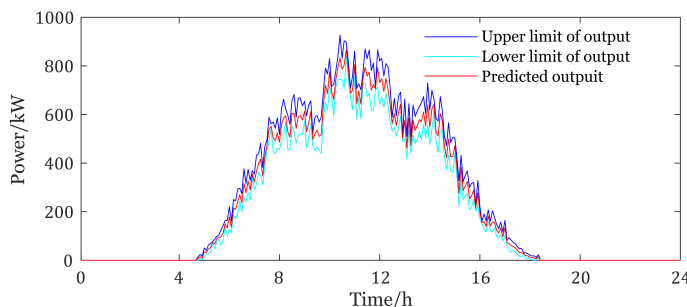


Figure 6.4: Output range of photovoltaic system.

Table 6.1: Setting of simulation parameters

Parameters	Values
$\lambda_{WT} / \lambda_{PV} / \lambda_{GT,1} / \lambda_{GT,2} / \lambda_{BESS}$	0.0408/0.0361/0.11837/0/0.0593
$P_{GT}^{\min} / P_{GT}^{\max} / P_{Ramp}^{\min} / P_{Ramp}^{\max} / P_{BESS}^{\max}$	500/4000/200/700/1000
$E_{BESS}^0 / E_{BESS}^{\min} / E_{BESS}^{\max}$	2000/1200/4000
η_{BESS} / κ	0.95/1
$\lambda_0^l / \lambda_0^g / \lambda_0^s / \eta^g / \lambda_{\Delta th}^d$	0.53/0.1922/0.3378/0.1228/0.03
$\bar{\lambda}^s / \bar{\lambda}^g / \bar{\lambda}^l$	0.53,0.38,0.25,0.12/0.27,0.22,0.15,0.08/0.8,0.6,0.4,0.2
$\underline{\lambda}^s / \underline{\lambda}^g / \underline{\lambda}^l$	0.69,0.53,0.38,0.25/0.31,0.27,0.22,0.15/1,0.8,0.6,0.4
$\begin{bmatrix} \rho_{11} & \rho_{12} & \rho_{13} & \rho_{14} \\ \rho_{21} & \rho_{22} & \rho_{23} & \rho_{24} \\ \rho_{31} & \rho_{32} & \rho_{33} & \rho_{34} \\ \rho_{41} & \rho_{42} & \rho_{43} & \rho_{44} \end{bmatrix}$	$\begin{bmatrix} -0.02 & 0.004 & 0.004 & 0.008 \\ 0.002 & -0.02 & 0.002 & 0.004 \\ 0.004 & 0.002 & -0.02 & 0.002 \\ 0.008 & 0.004 & 0.002 & -0.02 \end{bmatrix}$
N/MI	18/5
Q_{th2}	163198.74
ω	10%

By comparing scenarios 1 and 2, the impact of implementing ToU policy on the operational economics of deterministic power systems can be analyzed. By comparing scenarios 1 and 3, the impact of supply side uncertainty on the economics and robustness of power system operation without ToU policy can be analyzed. By comparing scenario 4 with 2 or 3, the impact of supply-demand uncertainty and ToU policy on the operation can be analyzed.

Table 6.2: Scenarios of simulation

Scenarios	Considered factors	
Scenario 1	ToU(N)	Supply-demand uncertainty (N)
Scenario 2	ToU(Y)	Supply-demand uncertainty (N)
Scenario 3	ToU (N)	Supply-demand uncertainty(Y)
Scenario 4	ToU(Y)	Supply-demand uncertainty(Y)

6.4.2 Results and analysis of scenario 1

In scenario 1, the supply-demand uncertainty of the new energy power system is not considered, and the ToU policy is not implemented. Specifically, power generation companies, grid companies, and power users follow a unified onto-grid prices, T-D prices, and selling prices for transactions. So, the optimization objective in this scenario is to minimize the operating costs of the power generation enterprise, as shown in (6.16).

$$\min C^s = \sum_{t=1}^T (C_{\text{GT}}(t) + C_{\text{BESS}}(t) + C_{\text{WT}}(t) + C_{\text{PV}}(t)) \quad (6.16)$$

The simulation results in this scenario can determine the benefits of each link without ToU policy. The output of power generation units on the supply side is shown in Figure 6.5.

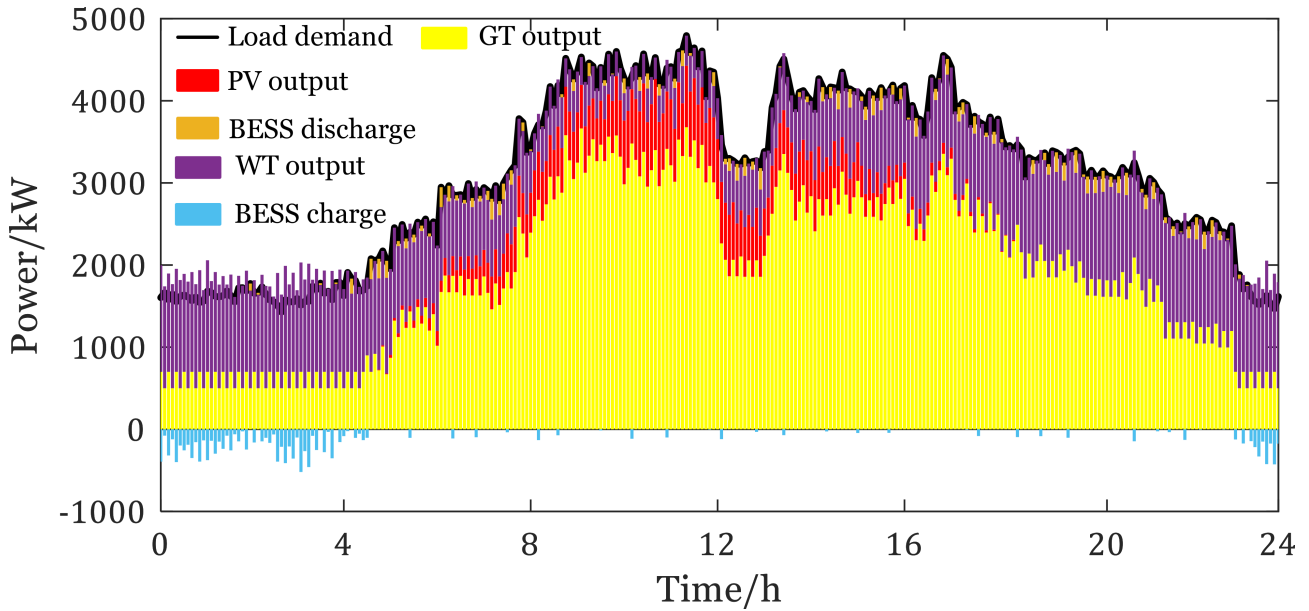


Figure 6.5: Output of power generation units on the supply side of scenario 1.

It can be seen that the majority of load demand is still met by gas turbines (GTs), especially between 05:00 and 19:00, which fully demonstrates the importance of GTs in maintaining stable and reliable operation of the power system. In the case where the output of WTs and PVs is fully absorbed (net load), the battery energy storage system (BESS) is responsible for absorbing excess electricity, especially between 23:00-04:00. When necessary, the BESS also discharges to meet the electricity needs of users.

Based on the unified peak-valley electricity prices for each link, the supply side benefits, grid side benefits, and user electricity cost are 18368.30 CNY, 5149.30 CNY, and 39324.54 CNY, respectively. From the above results, it can be seen that users pay more electricity bills than the benefits of supply side and grid side, because some of the electricity bills are used to pay government funds and other additional fees.

6.4.3 Results and analysis of scenario 2

In scenario 2, the system only considers implementing ToU policy. So, the optimization objective of this scenario is shown in (6.9). The simulation results of this scenario can determine the optimal benefits in a deterministic environment for each link. with considering ToU policy. The operational benefits of the system under different iteration times are shown in Figure 6.6.

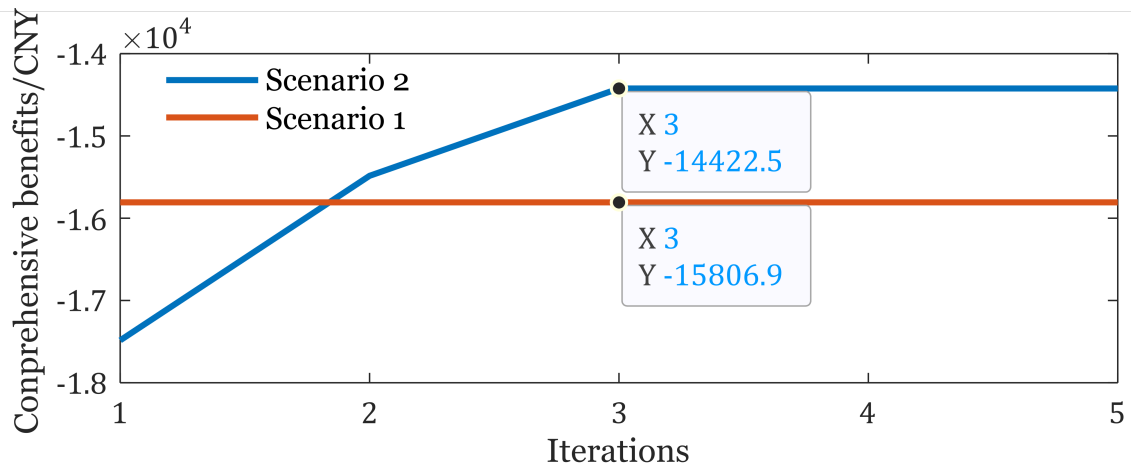


Figure 6.6: Curve of system operation benefits optimization.

Due to the global optimality of the CPLEX solver, the solution model based on the HOA and CPLEX only needs 3 iterations to converge. The convergence results indicate that in a deterministic environment, the optimal comprehensive benefits of scenario 1 and scenario 2 are -15806.90 CNY and -14422.50 CNY, respectively. Compared to scenario 1, the comprehensive benefits of the system after implementing ToU policy have increased by 1384.40 CNY, approximately 8.76%, showing significant improvement. The detailed profit comparison of each link is shown in Table 6.3.

Table 6.3: Changes in benefits of each link

System link benefits	Scenario 1	Scenario 2	Benefits change
supply side/power generation enterprises	18368.30 CNY	20401.35 CNY	+11.10%
grid side/grid enterprises	5149.30 CNY	5967.88 CNY	+15.90%
Demand side/electricity cost	39324.54 CNY	40791.70 CNY	-3.73%

It can be seen that after implementing ToU policy, the benefits on both the supply side and the grid side have increased by more than 10%. Despite the increase in electricity costs for users, the growth rate does not exceed 5%. Within the range of cost fluctuations, users effectively participated in demand response. The above changes in benefits demonstrate that ToU policy can effectively improve the economics of system operation. The optimized peak-valley tariff of each link is shown in Figure 6.7.

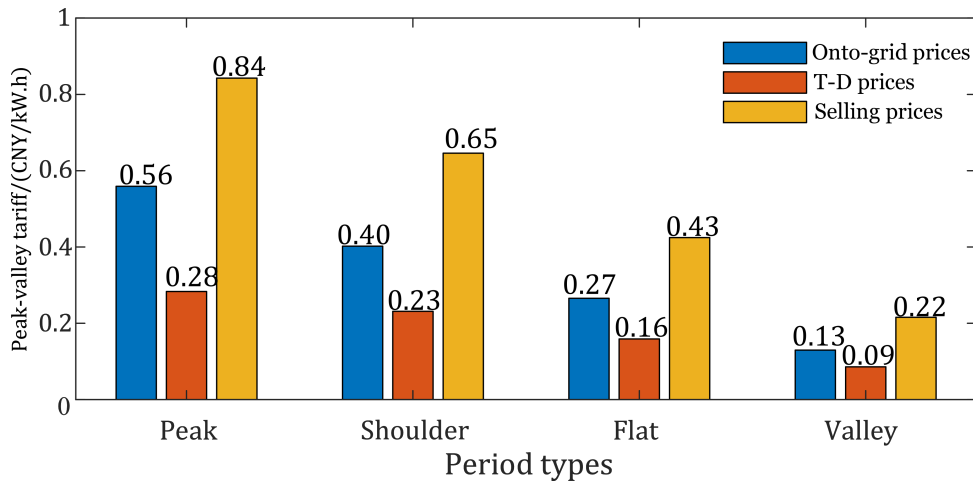


Figure 6.7: Peak-valley electricity prices of each link.

It can be concluded that the electricity prices of peak, flat, and valley periods satisfy the relationship that the selling price is equal to the sum of onto-grid price and T-D price. However, during the shoulder period, the electricity price satisfies the inequality relationship that the selling price is slightly greater than the sum. This conforms to the relaxed electricity price constraint (6.2). From the values of prices, it can be calculated that maintaining the peak-valley prices ratio between 3.11 times (T-D price) and 4.31 times (onto-grid price) can effectively prevent peak to valley inversion. The load curve after user participation in demand response is shown in Figure 6.8.

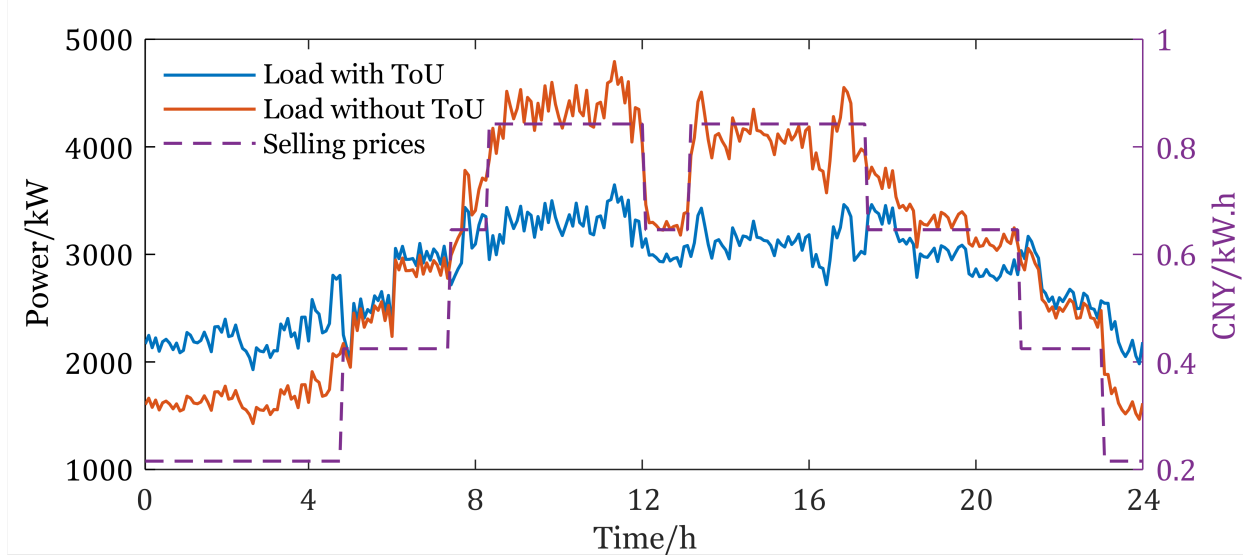


Figure 6.8: Load curve after time-of-use policy.

It can be seen that users actively participate in demand response and adjust their electricity plans according to the electricity prices at different times. The electricity consumption during valley and flat periods increases significantly, while the electricity consumption during shoulder and peak periods decreases accordingly. This significantly reduces the peak-valley difference of the load curve, making the curve smoother and more conducive to the stable operation of the power system. The load curve before demand response shows a significant bimodal characteristic, which is significantly weakened after the implementation of ToU policy. Based on the load curve comparison in Figure 6.8, the changes in electricity consumption during each period are shown in Table 6.4.

Table 6.4: Changes in electricity consumption during peak-valley periods

Period types	Before ToU (kW)	After ToU (kW)	Changes in electricity consumption
Peak	404669.44	307845.72	-23.93%
Shoulder	227357.59	206564.38	-9.15%
Flat	143587.71	148862.47	+3.67%
Valley	114752.20	155059.25	+35.13%

According to Table 6.4, after implementing ToU policy, the electricity consumption during peak and shoulder periods shows a decrease, while the electricity consumption during flat and valley periods increases accordingly. Among them, the decrease in electricity consumption

during peak periods is more significant, which is 2.62 times the decrease in shoulder periods; The increase in valley period is the most significant, which is 9.57 times the increase in flat period. This change indicates that a large amount of electricity consumption during peak periods has been transferred to valley periods. From this, it can be seen that ToU policy not only improves the comprehensive benefits of system operation, but also effectively shaves peak and fills valley, significantly reducing the peak-valley load difference and improving the stable and safe operation capability of the system. Based on the load curve after user participation in demand response, the output of each power source is shown in Figure 6.9.

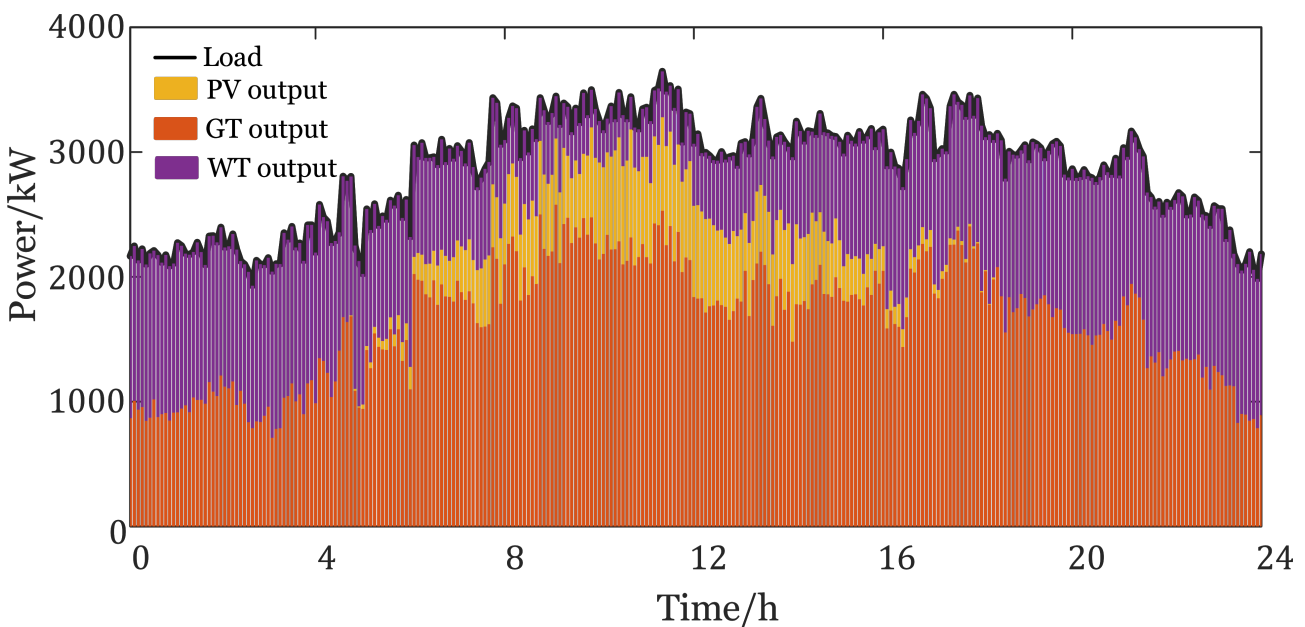


Figure 6.9: Output of each power generation unit in the supply side of scenario 2.

Compared with the output of the power generation units in scenario 1 (Figure 6.5), it can be seen that the BESS does not output in scenario 2. This is because after implementing ToU policy, the demand from users during valley hours increases, which can absorb the excess output of WTs and PVs. At the same time, the demand from users during peak hours decreases, and there is no need to discharge the BESS to meet user needs. In terms of the proportion of power generation, GTs still account for the majority of the output and are responsible for maintaining system stability.

6.4.4 Results and analysis of scenario 3

The new energy power system in scenario 3 does not consider ToU policy, so the system uncertainty only includes the uncertainty of wind and solar power output, which satisfies (5.16) and (5.17). The goal of this scenario is to minimize the operating cost of the power generation units, as shown in (6.16). Unlike scenario 1, the wind and solar power output is no longer fixed, but is set as a decision variable that follows a budget uncertainty set and participates in the optimization process. By adjusting the uncertainty, the operating cost of supply side can be obtained as shown in Figure 6.10.

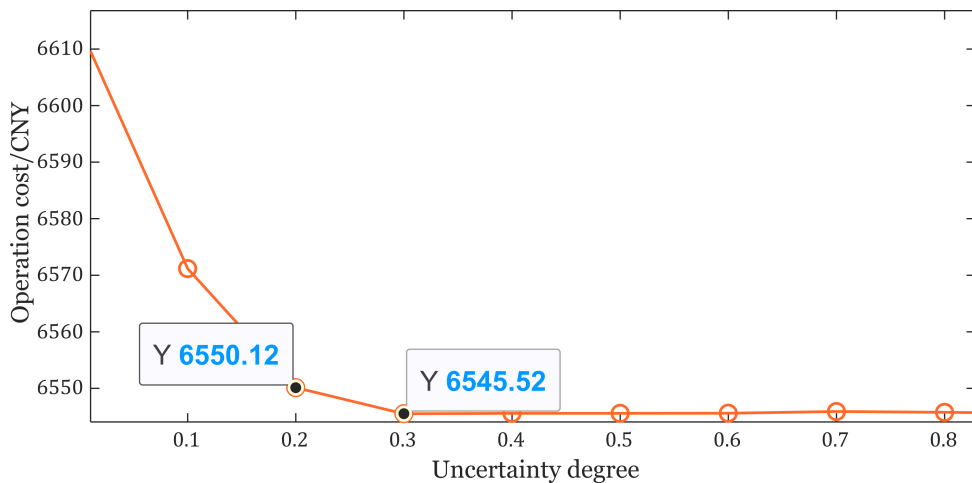


Figure 6.10: Supply side operating costs under different uncertainties.

Since the ToU policy is not considered, the onto-grid price of power generation enterprises is a constant, and the level of operating costs can reflect the level of benefits. From Figure 6.10, it can be seen that the greater the uncertainty Γ , the lower the operating cost on the supply side. When the uncertainty Γ is 0.4, the operating cost is the lowest, at 6545.52 CNY, and the corresponding benefit is 18518.31 CNY. This indicates that the larger the fluctuation range of wind and solar power output, the more natural resources can be utilized by the supply side to meet the electricity demand of users. However, this puts stricter requirements on power generation companies, including more accurate wind and solar forecasting capabilities, as well as stronger system robustness and anti-interference capabilities. The corresponding wind and solar power output prediction errors are shown in Figure 6.11, and the output of each power generation unit is shown in Figure 6.12.

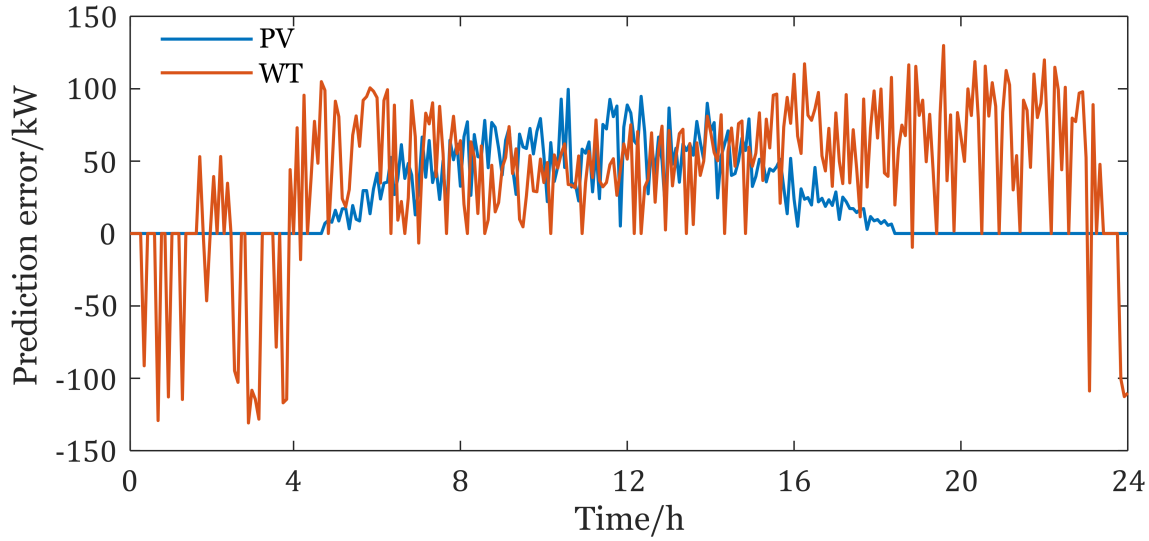


Figure 6.11: Prediction error of the output of WT and PV.

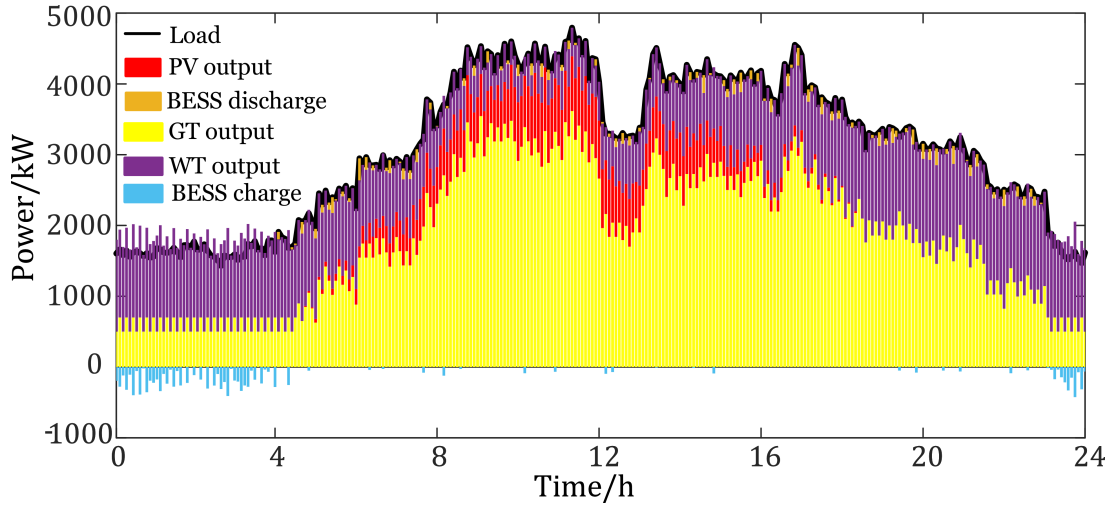


Figure 6.12: Output of each power generation unit with an uncertainty of 0.4.

From Figure 6.11, it can be seen that the fluctuation of the output prediction error of WTs is very obvious, with a maximum error of up to 135 kW. This indicates that the actual output of WTs varies at a high frequency in the upper and lower intervals of the predicted output. The fluctuation of the output prediction error of PVs is relatively small, with a maximum prediction error of no more than 100 kW, all operating in the interval above the predicted output. Due to the weak light intensity in the evening and early morning, PVs do not participate in power supply during these periods and have significant power generation characteristics, so their prediction difficulty is lower compared to WTs.

From Figure 6.12, it can be seen that compared with the operation of each power generation

unit in scenario 1 (Figure 6.5), the output proportion of GTs and BESS has not changed much. This is because the output proportion of WTs and PVs is not large, and the fluctuation of their output does not significantly affect the operation mode and trend of GTs and BESS. This further illustrates the importance of GTs in maintaining safe and stable system operation.

6.4.5 Results and analysis of scenario 4

The system in scenario 4 implements ToU policy and considers the uncertainty of supply side, which is the closest to the actual scheduling conditions. Adjusting the uncertainty of wind and solar power and the uncertainty of load response can obtain corresponding optimization results for analysis. In this scenario, the optimization objective is shown in (6.9), and the uncertainty of wind and solar power and load response satisfy (6.17).

$$\Gamma = \gamma \in \{25\%, 50\%, 75\%\} \quad (6.17)$$

The comprehensive benefits of the system under different uncertainties are shown in 6.13, and the ToU tariff of each link under different uncertainties are shown in Figures 6.14-6.16.

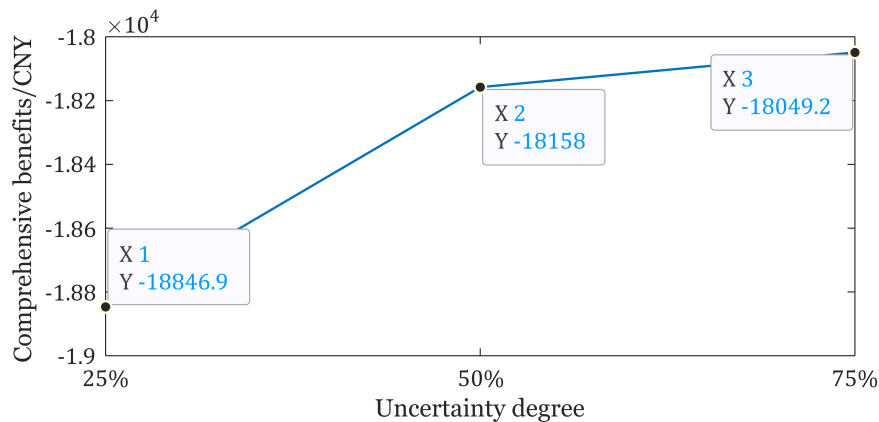


Figure 6.13: System comprehensive benefits under different uncertainties.

From Figure 6.13, it can be seen that as the uncertainty increases, the comprehensive benefits of the system continue to increase. This indicates that the new energy power system, under the conditions of accurate prediction of wind and solar resources and sufficient robustness, fully

absorbs the output of WTs and PVs to meet the load demand and improve operational economics. However, compared with the deterministic system comprehensive benefits of scenario 2 (Figure 6.6), it can be found that the system comprehensive benefits of scenario 4 are always lower than those of scenario 2, which means that the addition of supply-demand uncertainty makes the optimization results more conservative.

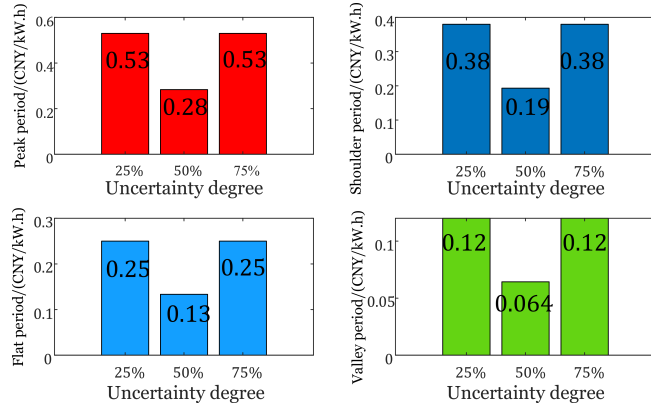


Figure 6.14: Peak-valley onto-grid prices under different uncertainties.

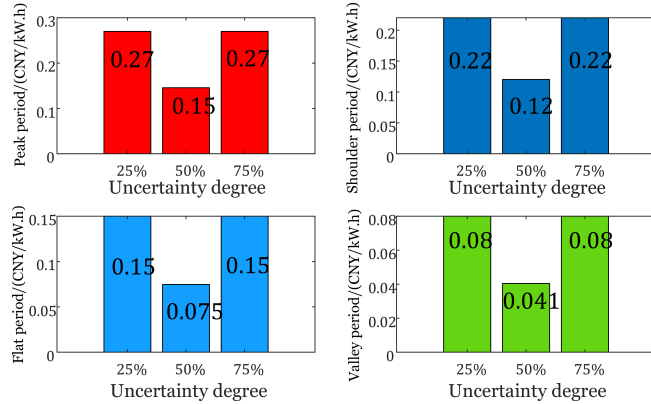


Figure 6.15: Peak-valley transmission-distribution prices under different uncertainties.

Analyzing the electricity prices in Figures 6.14-6.16, it can be seen that the peak-valley electricity prices in the three links have the same trend of change: decreasing first and then increasing with increasing uncertainty. However, the comprehensive benefits of system operation have been continuously increasing, indicating that the increase or decrease of electricity prices is not the only factor affecting the comprehensive benefits of system operation. The uncertainty of supply and demand not only reduces the operational benefits of the system, but also increases the difficulty of implementing Tou policy, that is, market transactions cannot

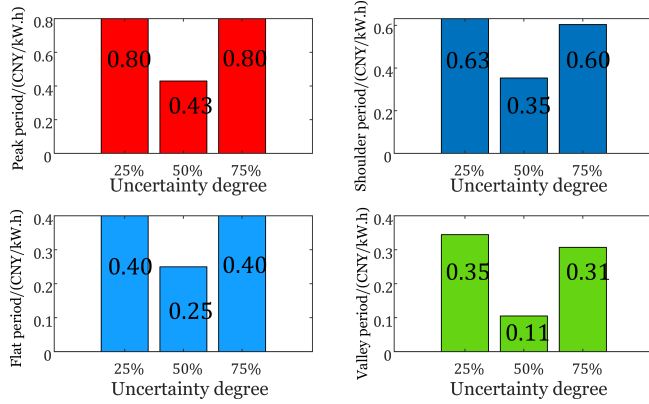


Figure 6.16: Peak-valley selling prices under different uncertainties.

be completely controlled based on ToU tariff. Even if almost the same peak-valley electricity prices are set (with uncertainties of 25% and 75%), users and power generation companies will make different decisions on electricity consumption and generation according to the specific situation, resulting in different comprehensive benefits of the system.

6.5 Chapter conclusion

This chapter aims to optimize the time-of-use electricity prices of the new energy power system for the benefits of power generation enterprises, power grid enterprises, and power users. The combination solution model based on hippopotamus optimization algorithm and CPLEX effectively transforms the original nonlinear programming into linear programming for solving. Constructing different simulation scenarios has proven that time-of-use policy can effectively narrow the supply-demand power gap and improve system economics. Power generation companies can reduce operating costs by consuming wind and solar power output, but this requires system robustness and accuracy in predicting wind and solar resources. The uncertainty of supply and demand will increase the difficulty of implementing time-of-use policy, making the optimization results more conservative.

Chapter 7

Conclusion

7.1 Summary of thesis achievements

Reasonable division of peak-valley periods and formulation of electricity prices are key to ensuring effective time-of-use policy. In response to the subjective judgment of peak-valley periods by humans, the traditional method of dividing periods is inefficient and lacks practical significance. This thesis proposes an improved K-Means clustering algorithm; When dividing the periods of small-scale load curves, it is easy to encounter the problem of rapid changes in period types. This thesis proposes a solution based on fuzzy subsethood; In response to the increasingly significant supply-demand uncertainty, this thesis proposes a time-of-use tariff optimization model for new energy power systems that considers supply-demand uncertainty, and explores the coupling relationship between uncertainties, time-of-use policy, and system economics. The main contributions of this thesis are four-fold:

- To establish a reasonable and effective mathematical model to divide the peak-valley periods of the load curve. The subjective experience judgment of human beings cannot fully reflect the characteristics of the load curve. Therefore, the model must fully explore the numerical relationship of load power. At the same time, the model must also consider its practical application significance. The improved membership function proposed in this

thesis is a modeling of prior knowledge to enhance the interpretability and effectiveness of the model.

- The traditional ToU period partitioning method based on clustering algorithm cannot handle the problem of rapid changes in time period types, so it is necessary to build a targeted correction model to deal with this problem. Rapid changes in period types can prevent users from developing reasonable plans to participate in demand response, resulting in poor implementation of ToU policy. The correction model based on fuzzy subsethood constructed in this thesis fully considers the characteristics and distribution of such abnormal periods, completes abnormal periods correction, and enables the results of the clustering algorithm to be used for subsequent optimization.
- The ToU electricity price optimization model for the new energy power system established in this thesis is a typical nonlinear programming problem, and the difficulty in solving it lies in how to incorporate the process of user participation in demand response into the optimization. This thesis proposes a combined solving model with hippopotamus optimization algorithm as the outer layer and CPLEX solver as the inner layer. By transferring their respective solutions, the difficult nonlinear programming problem is transformed into an easy to solve linear programming problem.
- The optimization model is solved and analyzed in different simulation scenarios to explore the impact of supply-demand uncertainty and ToU tariff on the economics of the power system operation. The implementation of ToU policy can significantly improve the comprehensive efficiency of system operation, while achieving the effect of peak shaving and valley filling, and improving the safety of system operation. However, the implementation effect of ToU policy is weakened by the uncertainty. If the system needs to utilize more wind and solar power, it must have more accurate prediction capabilities and robustness.

7.2 Future work

The time-of-use policy involves the complex interweaving of multiple interests and has a profound impact on the stable development of the social economy and the daily needs of people. Given the multitude and complexity of factors involved, it is necessary to further deepen and improve this mechanism in the future to ensure that it better serves social development. For the formulation of time-of-use policy, there are mainly the following directions that can be studied:

- Establish a peak-valley periods division model that considers multiple factors. In addition to exploring the numerical characteristics of load power, the results of periods division, methods for correcting abnormal time periods, and optimization goals such as improving user response enthusiasm, electricity usage satisfaction, and overall system operation economics can also be combined.
- Consider the design of time-of-use policy under multiple time scales. Dividing peak-valley periods on a small time scale and implementing peak-valley pricing can more clearly demonstrate the process of user participation in demand response, making it easier to control the uncertainty.
- Consider extreme and harsh operating scenarios in the optimization model. A typical two-stage robust optimization model is used for optimization scheduling, which can quantify the robustness of the system to the greatest extent possible. Its conservative optimization results can provide reference standards for scheduling personnel.
- Explore better nonlinear programming solution models. CPLEX can stabilize optimization objectives and achieve global optimality, but when combined with intelligent optimization algorithms to solve nonlinear problems, the entire solution model becomes full of randomness, meaning that the optimization results under the same conditions may differ, which can compromise the effectiveness of the optimization model. How to solve the nonlinear part of this type of problem is worth further research.

Bibliography

- [1] Z. Wang, U. Munawar, and R. Paranjape, “Stochastic optimization for residential demand response with unit commitment and time of use,” *IEEE Transactions on Industry Applications*, vol. 57, no. 2, pp. 1767–1778, 2020.
- [2] Y.-C. Hung and G. Michailidis, “Modeling and optimization of time-of-use electricity pricing systems,” *IEEE Transactions on Smart Grid*, vol. 10, no. 4, pp. 4116–4127, 2018.
- [3] Y. Hu, Y. Li, and L. Chen, “Multi-objective optimization of time-of-use price for tertiary industry based on generalized seasonal multi-model structure,” *IEEE Access*, vol. 7, pp. 89234–89244, 2019.
- [4] S. Park, Y. Jin, H. Song, and Y. Yoon, “Designing a critical peak pricing scheme for the profit maximization objective considering price responsiveness of customers,” *Energy*, vol. 83, pp. 521–531, 2015.
- [5] H. Li, H. Liu, J. Ma, and J. Wang, “Robust stochastic optimal dispatching of integrated electricity-gas-heat system considering generation-network-load uncertainties,” *International Journal of Electrical Power and Energy Systems*, vol. 157, p. 109868, 2024.
- [6] Y. Zhou, J. Chen, L. Zhang, Y. Zhang, C. Teng, and X. Huang, “Opportunity for developing ultra high voltage transmission technology under the emission peak, carbon neutrality and new infrastructure,” *High Voltage Engineering*, vol. 47, no. 07, pp. 2396–2408, 2021.
- [7] H. Li, L. Dong, and Y. Danyang, “Analysis and reflection on the development of power system towards the goal of carbon emission peak and carbon neutrality,” *Proceedings of the CSEE*, vol. 41, no. 18, pp. 6245–6259, 2021.

- [8] L. Wang, C. Hou, B. Ye, X. Wang, C. Yin, and H. Cong, "Optimal operation analysis of integrated community energy system considering the uncertainty of demand response," *IEEE Transactions on Power Systems*, vol. 36, no. 4, pp. 3681–3691, 2021.
- [9] L. Jia and L. Tong, "Dynamic pricing and distributed energy management for demand response," *IEEE Transactions on Smart Grid*, vol. 7, no. 2, pp. 1128–1136, 2016.
- [10] S. Maharjan, Q. Zhu, Y. Zhang, S. Gjessing, and T. Başar, "Demand response management in the smart grid in a large population regime," *IEEE Transactions on Smart Grid*, vol. 7, no. 1, pp. 189–199, 2015.
- [11] D. Ellman and Y. Xiao, "Incentives to manipulate demand response baselines with uncertain event schedules," *IEEE Transactions on Smart Grid*, vol. 12, no. 2, pp. 1358–1369, 2020.
- [12] A. Safdarian, M. Fotuhi-Firuzabad, and M. Lehtonen, "A medium-term decision model for discos: Forward contracting and tou pricing," *IEEE Transactions on Power systems*, vol. 30, no. 3, pp. 1143–1154, 2014.
- [13] Z. Tan, L. Pu, J. Wu, Y. Zhang, J. Yang, and S. Yang, "Time-of-use transmission and distribution price optimization model based on differential loading rate," *Systems Engineering-Theory and Practice*, vol. 39, no. 11, pp. 2945–2952, 2019.
- [14] G. Ma, Z. Cai, and P. Liu, "Power capacity optimization of microgrid with multiple subjects considering price incentive demand response," *Electric Power Automation Equipment*, vol. 39, no. 05, pp. 96–102+108, 2019.
- [15] H. Yang, Z. Gong, Y. Ma, L. Wang, and B. Dong, "Optimal two-stage dispatch method of household pv-bess integrated generation system under time-of-use electricity price," *International Journal of Electrical Power & Energy Systems*, vol. 123, p. 106244, 2020.
- [16] P. Liu, J. Yu, S. Fan, K. Bi, and Q. An, "Pev charging coordination using adaptive time-of-use tariffs to reduce wind energy curtailment," in *2018 IEEE Transportation Electrification Conference and Expo, Asia-Pacific (ITEC Asia-Pacific)*, pp. 1–5, IEEE, 2018.

- [17] M. Wu, "Economy of energy storage in electrified railway under time-of-use price policy," *Electric Power Automation Equipment*, vol. 40, no. 06, pp. 191–197+1–3, 2020.
- [18] D. Zhao, H. Wang, J. Huang, and X. Lin, "Time-of-use pricing for energy storage investment," *IEEE Transactions on Smart Grid*, vol. 13, no. 2, pp. 1165–1177, 2021.
- [19] Q. Ai, S. Fan, and L. Piao, "Optimal scheduling strategy for virtual power plants based on credibility theory," *Protection and control of modern power systems*, vol. 1, no. 1, pp. 1–8, 2016.
- [20] A. Z. Gabr, A. A. Helal, and N. H. Abbasy, "Multiobjective optimization of photo voltaic battery system sizing for grid-connected residential prosumers under time-of-use tariff structures," *IEEE Access*, vol. 9, pp. 74977–74988, 2021.
- [21] H. Yang, L. Wang, Y. Zhang, H.-M. Tai, Y. Ma, and M. Zhou, "Reliability evaluation of power system considering time of use electricity pricing," *IEEE Transactions on Power Systems*, vol. 34, no. 3, pp. 1991–2002, 2018.
- [22] B. Nan, C. Jiang, S. Dong, and C. Xu, "Day-ahead and intra-day coordinated optimal scheduling of integrated energy system considering uncertainties in source and load," *Power System Technology*, vol. 47, no. 09, pp. 3669–3683, 2023.
- [23] A. Safdarian, M. Fotuhi-Firuzabad, and F. Aminifar, "Compromising wind and solar energies from the power system adequacy viewpoint," *IEEE Transactions on Power Systems*, vol. 27, no. 4, pp. 2368–2376, 2012.
- [24] B. Sang, T. Zhang, Y. Liu, L. Liu, J. Zhu, and R. Wang, "Two-stage robust optimal scheduling of grid-connected microgrid under expected scenarios," *Proceedings of the CSEE*, vol. 40, no. 19, pp. 6161–6173, 2020.
- [25] Y. Wu, B. Zhang, G. Yuan, H. Yi, and R. Lv, "Optimal configuration of micro-grid considering uncertainties of electric vehicles and pv/wind sources," *Electrical Measurement and Instrumentation*, vol. 53, no. 16, pp. 39–44, 2016.

- [26] M. Cui, T. Feng, and L. Liu, "Integration and development of blockchain and renewable energy under double carbon target," *Smart Power*, vol. 52, no. 02, pp. 17–24, 2024.
- [27] Y. Mi, H. Zhao, Q. Fu, S. Ma, P. Cai, and M. Yuan, "Two-level game optimal operation of regional integrated energy system considering wind and solar uncertainty and carbon trading," *Power System Technology*, vol. 47, no. 06, pp. 2174–2188, 2023.
- [28] Y. Liu, L. Guo, and C. Wang, "Economic dispatch of microgrid based on two stage robust optimization," *Proceedings of the CSEE*, vol. 38, no. 14, pp. 4013–4022+4307, 2018.
- [29] Q. Xu, D. Wang, W. Dai, and K. Zhang, "Virtual synchronous machine transformation of inverter air conditioning load and its participation in microgrid interactive control," *Electric Power Automation Equipment*, vol. 40, no. 03, pp. 8–14, 2020.
- [30] P. Wang, Y. Ma, Z. Ling, and G. Luo, "A modified k-means clustering algorithm based on fmf-gs-dd.," *Engineering Letters*, vol. 31, no. 4, 2023.
- [31] P. Wang, Y. Ma, Z. Ling, and G. Luo, "Peak-valley period partition and abnormal time correction for time-of-use tariffs under daily load curves based on improved fuzzy c-means," *IET Generation, Transmission and Distribution*, vol. 17, no. 24, pp. 5396–5409, 2023.
- [32] X. Zhu and Z. Liao, "The measure of fuzzy ideals of lattices," *J. Zhengzhou Univ. (Nat. Sci. Ed.)*, vol. 51, no. 02, pp. 107–112, 2019.
- [33] A. Chen, H. Hua, P. Li, and Y. Su, "Optimal operation of ac/dc hybrid micro-grid based on real-time price mechanism," *Power System Protection and Control*, vol. 45, no. 07, pp. 13–20, 2017.
- [34] L. Shi, C. Wang, L. Yao, Y. Ni, and M. Bazargan, "Optimal power flow solution incorporating wind power," *IEEE Systems Journal*, vol. 6, no. 2, pp. 233–241, 2011.
- [35] L. Li, Y. Yu, X. Yuan, W. Xiong, Y. Xu, and H. Liu, "Power supply restoration method for flexible interconnected distribution networks with opportunity constraints," *Power System and Automation*, vol. 45, no. 05, pp. 38–41, 2023.

- [36] P. Wang, R. Cao, and W. Ye, “Analysis of the influence of the spatial-temporal characteristics of wind power and photovoltaics on the economic dispatch of independent microgrids,” in *Annual Conference of China Electrotechnical Society*, pp. 754–761, Springer, 2022.
- [37] M. Dehghani Filabadi and H. Mahmoudzadeh, “Effective budget of uncertainty for classes of robust optimization,” *INFORMS Journal on Optimization*, vol. 4, no. 3, pp. 249–277, 2022.
- [38] J. Huang, X. Yu, D. Zhao, Y. Fan, H. Chen, S. Yu, and Y. Li, “Bi-layer optimization model of peak-valley prices and peak-valley periods considering benefits of source-grid-load,” *Electric Power Automation Equipment*, vol. 44, no. 06, pp. 217–224, 2024.
- [39] M. H. Amiri, N. Mehrabi Hashjin, M. Montazeri, S. Mirjalili, and N. Khodadadi, “Hippopotamus optimization algorithm: a novel nature-inspired optimization algorithm,” *Scientific Reports*, vol. 14, no. 1, p. 5032, 2024.